Controlled production of bacterial outer membrane vesicles in intestine by orally administered bacteria as an effective tumor vaccine

Yale Yue
National Center for Nanoscience and Technology
Jiaqi Xu
National Center for Nanoscience and Technology
Yao Li
National Center for Nanoscience and Technology
Keman Cheng
National Center for Nanoscience and Technology
Qingqing Feng
National Center for Nanoscience and Technology
Xiaotu Ma
National Center for Nanoscience and Technology
Nana Ma
National Center for Nanoscience and Technology
Tianjiao Zhang
National Center for Nanoscience and Technology
Xinwei Wang
National Center for Nanoscience and Technology
Xiao Zhao
National Center for Nanoscience and Technology
Guangjun Nie (niegj@nanoctr.cn)
National Center for Nanoscience and Technology https://orcid.org/0000-0001-5040-9793

Article

Keywords: Gastrointestinal Environment, Intestinal Epithelial Barriers, Intestinal Commensal Bacteria, Arabinose-inducible Promoter, Dendritic Cell Maturation

Posted Date: July 14th, 2021

DOI: https://doi.org/10.21203/rs.3.rs-690237/v1

Version of Record: A version of this preprint was published at Nature Biomedical Engineering on May 2nd, 2022. See the published version at https://doi.org/10.1038/s41551-022-00886-2.

Controlled production of bacterial outer membrane vesicles in intestine by orally administered bacteria as an effective tumor vaccine

Yale Yue[1,2,3&], Jiaqi Xu[1,2&], Yao Li[1&], Keman Cheng[1], Qingqing Feng[1], Xiaotu Ma[1], Nana Ma[1], Tianjiao Zhang[1], Xinwei Wang[1], Xiao Zhao[1,4*], Guangjun Nie[1,2*]

[1]CAS Key Laboratory for Biomedical Effects of Nanomaterials and Nanosafety, CAS Center for Excellence in Nanoscience, National Center for Nanoscience and Technology, China, No.11 Zhongguancun Beiyitiao, Beijing 100190, China

[2]Center of Materials Science and Optoelectronics Engineering, University of Chinese Academy of Sciences, Beijing 100049, China

[3]School of Basic Medical Sciences, Zhengzhou University, Zhengzhou 450001, China

[4]Key Laboratory of Genetic Network Biology, Institute of Genetics and Developmental Biology, Chinese Academy of Sciences, Beijing, 100101, China

[&]These authors contributed equally

*Corresponding authors, zhaox@nanoctr.cn; niegj@nanoctr.cn

The orally administered tumor vaccines are still limited, and the major challenges are the complex gastrointestinal environment and intestinal epithelial barriers. Here, we present an effective tumor vaccine based on the OMVs which are generated by orally administered genetically engineered bacteria in intestine. A tumor antigen was fused with the surface protein ClyA on OMVs, whose expression was controlled by an arabinose-inducible promoter. Through oral administration of the modified bacteria and arabinose, *in situ* controllable production of OMVs loaded with tumor antigen in the intestine was achieved. The OMV-based tumor vaccine not only overcame the intestinal epithelial barriers to reach the immune cells in the lamina propria, but also stimulated dendritic cell maturation to facilitate a potent antitumor adaptive immunity. The oral bacteria generated OMV-based tumor vaccine significantly inhibited the lung metastatic melanoma and subcutaneous colon cancer in mouse models. Furthermore, a robust immune memory was generated, offering long-term protection against tumor challenge. Our work provides a proof-of-concept for oral bacteria generated OMV-based tumor vaccine that may be further translated into clinical use.

As personalized tumor immunotherapy, tumor vaccines involve using tumor antigens produced by genetic mutations to activate specific cytotoxic T cell lymphocytes (CTLs) that then attack tumor cells [1-3]. Currently, the majority of tumor vaccines in clinical trials are administered by either intramuscular or subcutaneous injection, in which the immune stimulation is confined to the limited number of draining lymph nodes [4,5]. Since the intestine acts as the largest immune organ, containing about 70% of the body's immune cells, oral administration of a tumor vaccine is a promising alternative option to elicit robust antitumor immune responses [6,7]. In addition, oral administration is met with better patient compliance and lower medical costs than injection [4,8]. However, oral tumor vaccines have been limited due to the challenges of the complex gastrointestinal environment and intestinal epithelial barriers. An ideal oral tumor vaccine must tolerate the gastrointestinal environment to reach the intestinal tract and overcome the intestinal epithelial barriers to interact with the

abundant immune cells in the lamina prima [9]. In the field of prophylactic vaccines for infectious diseases, attenuated live vaccines are applied orally in the clinic, such as oral poliovirus vaccine, therefore effectively overcoming the intestinal epithelial barriers, exploiting the natural features of microbes [4,10]. However, this approach is not suitable for an oral tumor vaccine, because tumor cells do not possess the ability to penetrate the epithelial barriers. In addition, the attenuated live vaccines still carry the potential risk of infection and transmission [10]. Since the development of next-generation vaccines focuses on safer and more efficient candidates, some synthetic carriers have been developed for oral vaccine delivery, such as liposomes, polymeric nanoparticles, and oil droplets, however their effectiveness is still suboptimal, and a new paradigm of oral vaccine technology is in urgent need [4,10-14].

Using engineered microbes for delivering therapeutic agents and treating disease has received increasing attention in recent years [15-17]. In consideration of the numerous symbiotic bacteria present in the intestine, engineered bacteria have the potential to tolerate the gastrointestinal environment and behave as artificial robots in the intestine [18-20]. Indeed, previous studies have demonstrated that orally administered programmed bacteria or modified probiotics can recognize colon cancer tissue in the intestine and enable local delivery of therapeutic agents, thereby promoting tumor regression [21,22]. Intriguingly, gut bacteria release messenger particles, known as outer membrane vesicles (OMVs), that interact with the host immune system [23,24]. OMVs are natural nanoparticles, secreted by Gram-negative bacteria, which can activate the innate immune system due to their abundance of pathogen-associated molecular patterns (PAMPs) [25-27]. The OMVs released by intestinal bacteria possess the ability to penetrate the intestinal epithelial barriers and interact with immune cells in the lamina propria, especially dendritic cells (DCs), resulting in immune regulation [28,29].

Addressing the technical obstacles of oral tumor vaccines and taking advantage of the biological characteristics of intestinal symbiotic bacteria, herein we report a genetically engineered bacteria-derived oral tumor vaccine (**Figure 1**). First, we fused the tumor antigen (Ag) and Fc fragment of mouse IgG (mFc) to the C-terminal of the surface protein, ClyA, of OMVs (ClyA-Ag-mFc). We hypothesized that the mFc would enhance the recognition and uptake of OMVs by DCs via the interaction between Fc and the neonatal Fc receptor (FcRn) [30-32]. In addition, in order to realize the strict vaccination route and avoid immune tolerance caused by long-term antigen stimulation, we introduced an arabinose-inducible promoter to control the fusion protein expression [33,34]. Through oral administration of the modified bacteria and expression inducer arabinose (Ara), we achieved *in situ* controllable production of OMVs loaded with tumor antigen (OMV-Ag-mFc) in the intestine. These OMV-Ag-mFc effectively crossed the intestinal epithelial barriers and were taken up by DCs in the lamina propria, followed by lymph node drainage and tumor antigen presentation. Tumor antigen-specific immune activation led to a significant inhibition of tumor growth and resistance to tumor challenge in multiple murine cancer models.

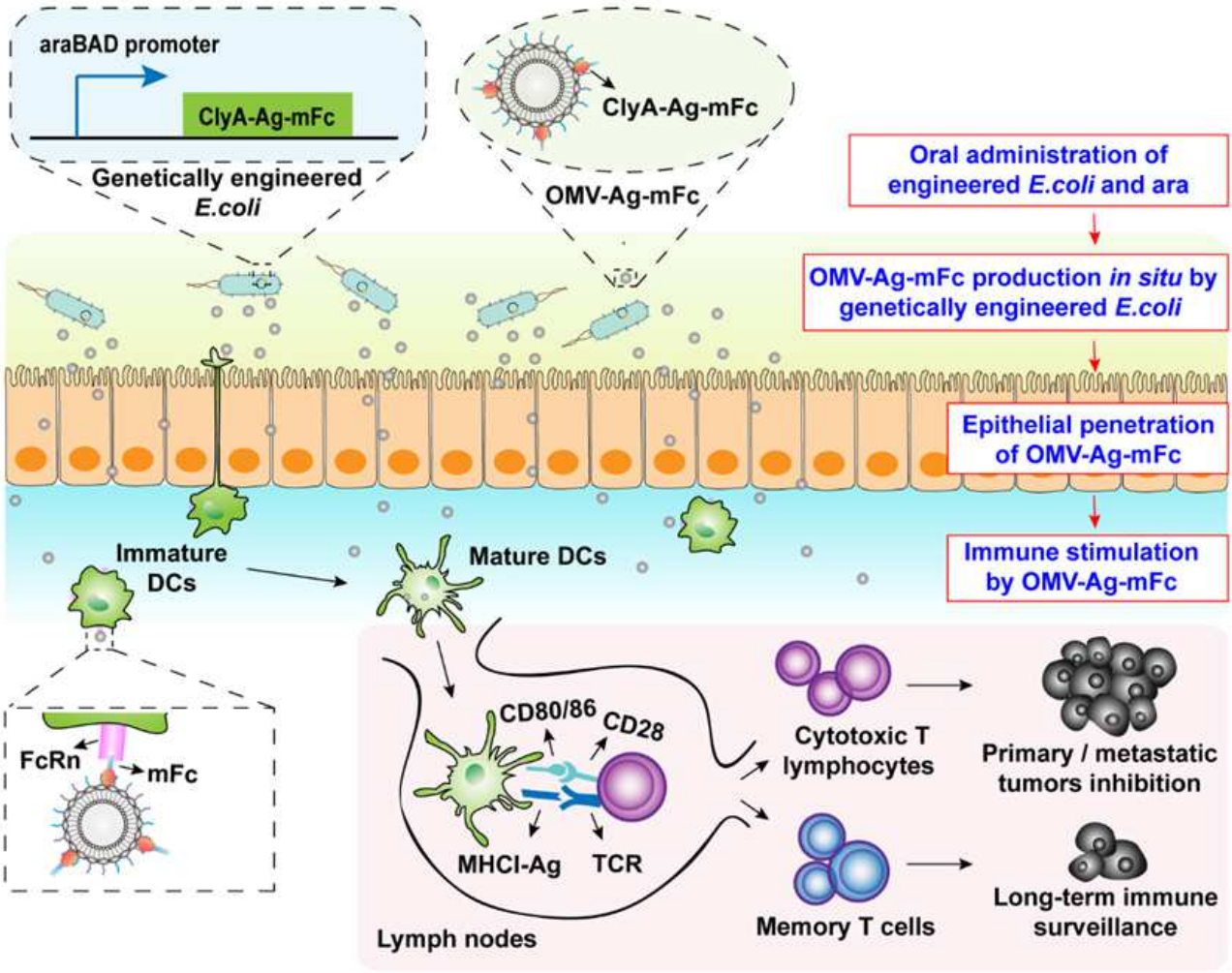

Fig. 1 | Schematic illustration of the genetically engineered bacteria-derived OMV-based oral tumor vaccine. Engineered *E. coli* were obtained by transformation with a plasmid expressing ClyA (a surface protein on OMVs) fused with a tumor antigen and Fc fragment of mouse IgG (ClyA-Ag-mFc). An arabinose-inducible promoter (araBAD) was introduced to control the fusion protein expression. After oral administration of engineered *E. coli* and expression inducer, Ara, OMVs loaded with tumor antigen (OMV-Ag-mFc) are produced in the intestine of mice. By virtue of the OMVs' natural behavior, OMV-Ag-mFc effectively penetrate the intestinal epithelial barriers, and are recognized and taken up by DCs in lamina propria via the interaction between mFc and FcRn. Due to the amount of PAMPs in OMVs, DCs rapidly mature, which then drain to the lymph node and complete tumor antigen presentation, resulting in expansion of antigen-specific cytotoxic T lymphocytes and memory T cells.

Results

Biodistribution analysis of engineered *E. coli* after oral administration *in vivo*

To visualize the biodistribution of the bacteria, we first engineered *E. coli* (Top10 strain) to express luciferase fused with an HA tag (Luc-HA) under the control of an araBAD promoter, which is activated by Ara (pBAD-Luc-HA). As shown in **Figure 2a**, using western blot analysis, the Luc-HA expression was detected only in the pBAD-Luc-HA *E. coli* after Ara induction. After adding the luciferase substrate (fluorescein potassium), fluorescence was observed in the pBAD-Luc-HA *E. coli* group after adding Ara (**Figure 2a**). Next, we administered the engineered *E. coli* orally to mice, followed by oral Ara. After 12 h, the gastrointestinal tissues from different locations and feces were collected for bioluminescence detection. Bioluminescent signals were observed in the contents of the cecum, colon, and feces from mice in the pBAD-Luc-HA *E. coli* + Ara group

(**Figure 2b**). These results demonstrate that the orally administered, engineered *E. coli* were able to reach the intestine and tolerate the intestinal environment, which ensured the successful expression of the target fusion protein when Ara was also taken orally. In addition, the extent of the induction in the engineered bacteria was Ara concentration-dependent, and 20 g/L of Ara was chosen for the further experiments (**Figure 2c**).

Next, we evaluated the biodistribution and pharmacokinetics of the engineered *E. coli*. As shown in **Figures 2d and 2e**, after oral administration with pBAD-Luc-HA *E. coli* and Ara, the bioluminescent signals mainly appeared in the cecum at 2 h after administration, and gradually moved to the colon within 12 h. After 24 h, the bioluminescent signal became weak, due to the metabolic clearance of the bacteria, which is important for the biosafety of an oral vaccine.

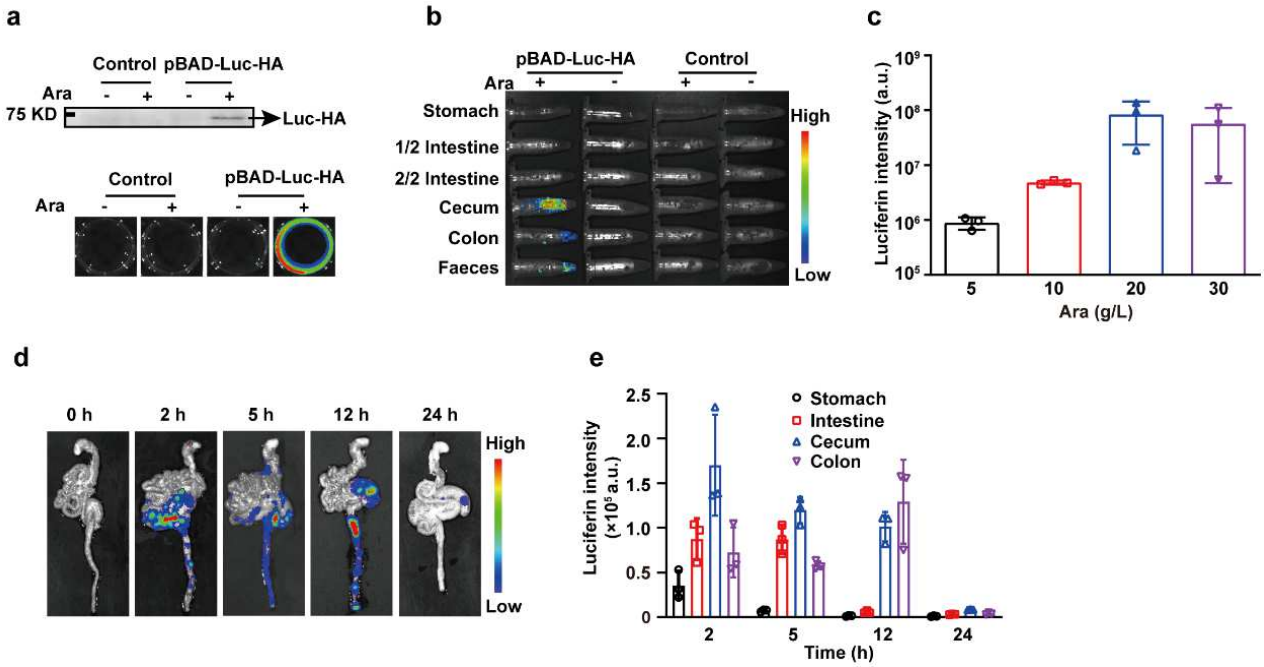

Figure 2 I Biodistribution analysis of engineered *E. coli* after oral administration. a, Representative western blot analysis and *in vitro* bioluminescence images of engineered *E. coli* expressing luciferase fused with the HA tag (Luc-HA) under the control of Ara induction. **b,** *In vivo* bioluminescence images of intestinal contents at 12 h after oral administration of engineered *E. coli* with or without oral Ara solution. **c,** Optimization of Ara concentration for *in vivo* induction. After oral administration of pBAD-Luc-HA *E. coli*, mice were provided the indicated concentrations of Ara. Feces were collected after 12 h and the bioluminescence intensities of luciferase were analyzed (n = 3). **d-e,** The biodistribution and pharmacokinetics of pBAD-Luc-HA *E. coli in vivo*. The biodistribution of pBAD-Luc-HA *E. coli* in the gastrointestinal tract at different timepoints post oral administration with 20 g/L Ara was analyzed using *in vivo* bioluminescence imaging (**d**). The bioluminescence intensities of luciferase in different locations along the gastrointestinal tract were quantified (n = 3; **e**). Data are presented as the mean ± SD.

Epithelial penetration and immune stimulation of the oral vaccine

To investigate whether the oral vaccine was able to stimulate the immune system, we fused an epitope of ovalbumin (OVA) [$OVA_{257-264}$ (SIINFEKL)] and/or mFc to the C-terminal of the surface protein, ClyA, of OMVs to generate ClyA-mFc, ClyA-OVA and ClyA-OVA-mFc, all of which were labelled with an HA tag. Using western blot analysis to evaluate the HA-tag expression, we verified the Ara-controlled expression of these fusion proteins in the engineered bacteria and their secreted OMVs (**Supplementary figure 1a**). In the transmission

electron microscopy (TEM) observation, all OMVs exhibited a uniform spherical morphology with a bilayer structure (**Supplementary figure 1b**). The diameters of the OMVs detected by dynamic light scattering (DLS) in control, ClyA-mFc, ClyA-OVA and ClyA-OVA-mFc groups were 21.5, 22.0, 23.9 and 30.3 nm, respectively (**Supplementary figure 1c**).

We proceeded to investigate the ability of OMVs to penetrate the intestinal epithelial barriers *in vitro* and *in vivo*. To this end, we co-cultured colon cancer Caco-2 and HT29 cells in the upper chamber of a transwell system for 21 days to simulate the intestinal epithelial barriers [35]. Next, DC2.4 cells were seeded in the lower chamber, and OMVs from different engineered bacteria were added into the upper chamber (**Supplementary figure 2a**). The percentages of mature DCs (using the co-stimulatory molecules, $CD80^+CD86^+$, as markers) were analyzed by flow cytometry after 12 h. OMVs effectively penetrated the epithelial barriers and activated DCs in the lower chamber. As expected, OMVs expressing mFc (ClyA-mFc and ClyA-OVA-mFc) exhibited a higher activation efficiency (**Supplementary figure 2b**). Next, we performed an enema experiment to examine the penetration ability of OMVs *in vivo*. The mice were anesthetized, the colon was ligated, and different OMVs were injected into the ligated intestinal cavity. After a 2 h incubation, the ligated colon was excised for immunofluorescence analysis. OMVs were detected using an anti-HA antibody (red), and DCs were labelled with an anti-CD11c antibody (green). As shown in **Figures 3a and 3b**, there was apparent penetration of the intestinal epithelial barriers by the OMVs in ClyA-mFc, ClyA-OVA and ClyA-OVA-mFc groups. Additionally, OMVs with mFc exhibited greater penetration (**Figure 3b**) and DC affinity (**Figure 3a**, white arrows) than OMVs without mFc. In summary, the OMVs secreted by engineered *E. coli* were able to penetrate the intestinal epithelial barriers, and the ClyA fusion with mFc was beneficial for this process.

We next examined the ability of the oral bacteria-derived vaccine to stimulate the immune system *in vivo*. Mice received vaccination through oral administration with different engineered bacteria, and consumed the Ara solution for 12 h. After a single vaccination, the immune cells in the lamina propria were isolated and analyzed by flow cytometry (**Supplementary figure 3**). As shown in **Figure 3c**, compared with the oral phosphate buffered saline (PBS) group, the proportions of $CD80^+CD86^+$ cells in $CD11c^+$ DCs significantly increased in all the oral bacteria-derived vaccine groups, even in the group that received the oral ClyA-OVA-mFc bacteria without Ara induction [ClyA-OVA-mFc (-Ara)]. The proportions of $CD80^+CD86^+$ cells in $CD11c^+$ DCs were higher in the oral ClyA-mFc and ClyA-OVA-mFc vaccine groups than that in the oral ClyA-OVA vaccine group (**Figure 3c**), which may be due to the mFc-mediated epithelial penetration enhancement. These results suggest that the immune cells in the lamina propria of mice tolerate the intrinsic symbiotic bacteria, while the orally administered foreign bacteria stimulated the DCs in the lamina propria via an OMV-mediated mechanism. We studied the antigen-specific immune responses after 3 rounds of immunization with different oral bacteria-derived vaccines (days 0, 3 and 8). On day 12, the splenocytes were collected and stimulated with an $OVA_{257–264}$ antigen peptide. As shown in **Figure 3d and Supplementary figure 4**, the oral ClyA-OVA-mFc vaccination stimulated the highest number of antigen-specific T cells (OVA $tetramer^+$ in $CD3^+CD8^+$ cells). Compared with that in the oral ClyA-OVA-mFc vaccine group, the markedly lower number of antigen-specific T cells in the oral ClyA-OVA-mFc (-Ara) vaccine group verifies that the immune stimulation of this oral bacteria-derived vaccine could be controlled by oral administration of Ara (**Figure 3d**). We also evaluated the cytotoxic effects of these collected splenocytes on ovalbumin-expressing melanoma B16 (B16-OVA) and colon cancer

MC38 cells. As shown in **Figure 3e**, the splenocytes from the ClyA-OVA-mFc vaccine group exhibited a stronger cytotoxic effect against B16-OVA cells than those from the ClyA-OVA vaccine group, indicating the importance of the epithelial penetration enhancement by mFc modification. The cytotoxic effect in all groups disappeared when using MC38 cells, which do not express the OVA antigen, thus demonstrating the antigen specificity of the immune stimulation by the oral bacteria-derived vaccine (**Figure 3f**). Taken together, the novel oral vaccine was able to produce OMVs loaded with tumor antigen in the intestine under the control of Ara. The *in situ* OMVs vaccine could penetrate the intestinal epithelial barriers and activate antigen-specific T cells against tumor cells.

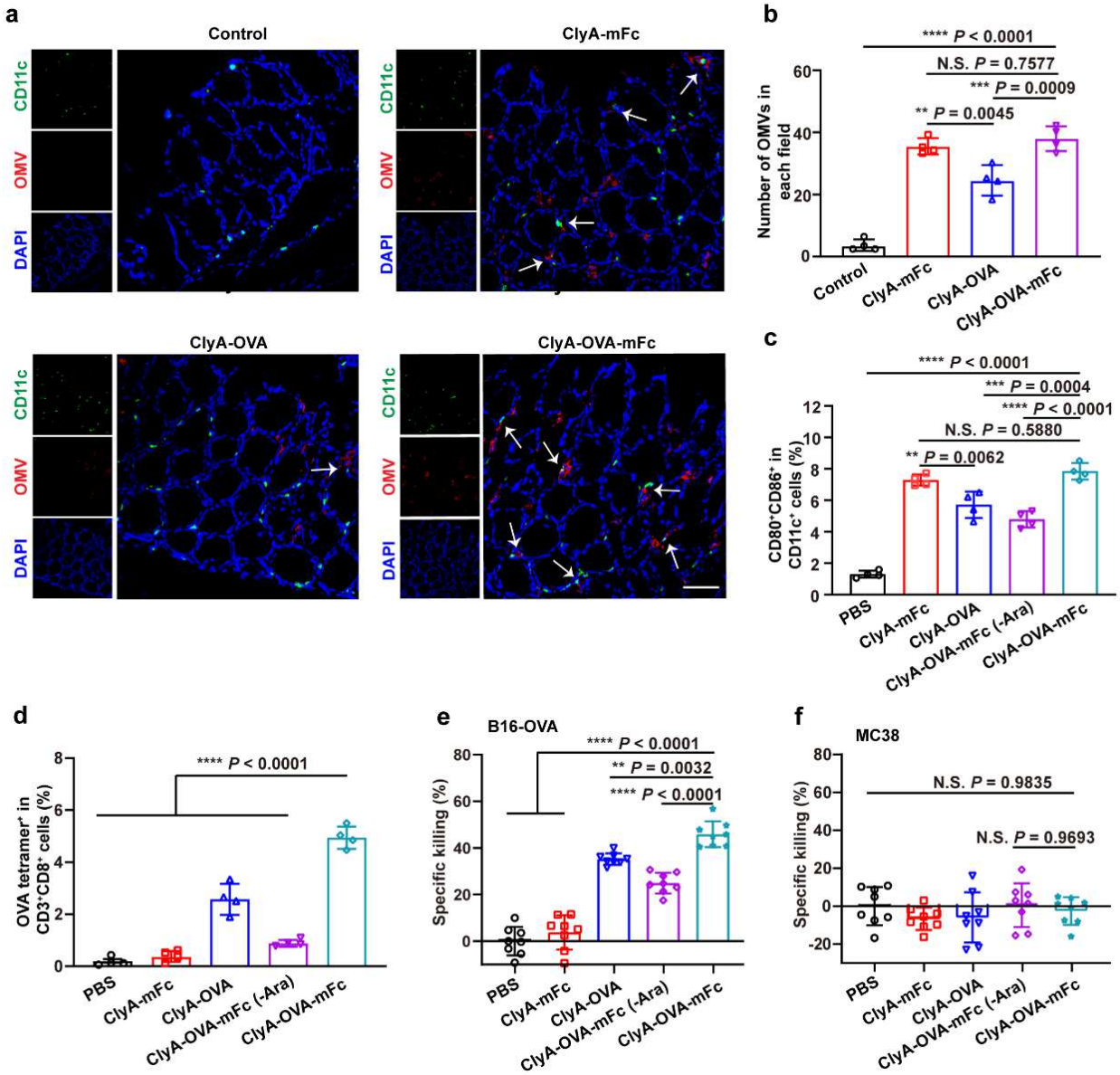

Figure 3 l Epithelial penetration and immune stimulation analysis of the oral vaccines. a-b, Analysis of epithelial penetration of OMVs from different the indicated engineered bacterial vaccines *in vivo*. Mice were anesthetized, the colon was ligated and different OMVs were injected into the ligated intestinal cavity. After a 2 h incubation, the ligated colon was excised for immunofluorescence analysis (**a**). The cell nucleus was stained with DAPI (blue), OMVs were detected using an anti-HA antibody (red) and DCs were labelled with an anti-CD11c antibody (green). The white arrows indicate the interaction between OMVs and DCs. The numbers of penetrating HA-labelled OMVs in each area were quantified (n = 4; **b**). Scale bar, 100 μm. **c-f,** Immune stimulation analysis of the indicated oral vaccines. C57BL/6 mice were immunized with an oral vaccine or PBS on days 0, 3 and 8. On day 1, after a single vaccination, the immune cells in the lamina propria were isolated.

The percentages of $CD80^+CD86^+$ in $CD11c^+$ cells were analyzed using flow cytometry (n = 4; **c**). On day 12, after 3 vaccinations, the splenocytes were collected and re-challenged with OVA peptide. The percentages of OVA $tetramer^+$ in $CD3^+CD8^+$ cells were also analyzed by flow cytometry (n = 4; **d**). The cytotoxic effects of splenocytes on B16-OVA cells (with OVA antigen; **e**) and MC38 cells that lack the OVA antigen (**f**) were analyzed using the CCK-8 assay (n = 8). The data are presented as the mean ± SD and were analyzed by one-way analysis of variance (ANOVA) with GraphPad Prism software. N.S., no significance; *, $P < 0.05$; **, $P < 0.01$; ***, $P < 0.001$; ****, $P < 0.0001$.

Antitumor effects in a lung metastatic melanoma model

Considering that the majority of immune cells in the entire immune system reside in the intestine, a specific immune stimulation in the intestine is expected to elicit a robust antitumor effect [17,36]. To evaluate the antitumor effects of the oral vaccine on metastatic melanoma, we inoculated mice intravenously with B16-OVA cells on day 0, and immunized the animals orally with the various oral vaccine formulations or PBS (control) on days 3, 6 and 11 (**Figure 4a**). The lungs were collected and photographed on day 17 (**Supplementary figure 5**). In the oral ClyA-mFc and oral ClyA-OVA-mFc (-Ara) vaccine groups, there was no significant reduction in lung metastases compared with that in the oral PBS group, likely due to the lack of OVA antigen and inducer in the vaccine systems (**Figure 4b**). In contrast, vaccination with the oral ClyA-OVA vaccine suppressed about 60% of lung metastases, while the lung metastases were almost eliminated in the oral ClyA-OVA-mFc vaccine group (**Figure 4b**).

We also assessed the degree of activation of antigen-specific T cells in the splenocytes of immunized mice by flow cytometry, using IFN-γ and OVA tetramer as markers of activation and antigen specificity, respectively [37]. As shown in **Figure 4c-4f**, the proportions of either IFN-γ^+ or OVA $tetramer^+$ in $CD3^+CD8^+$ T cells in splenocytes re-stimulated with $OVA_{257–264}$ antigen peptide were the highest in the oral ClyA-OVA-mFc vaccine group. In addition, the levels of lung-infiltrating $CD8^+$ CTLs were also the highest in the oral ClyA-OVA-mFc vaccine group (**Figure 4g and 4h**). These results demonstrate that the ClyA- OVA-mFc is an effective oral tumor vaccine that can successfully elicit antitumor immunity.

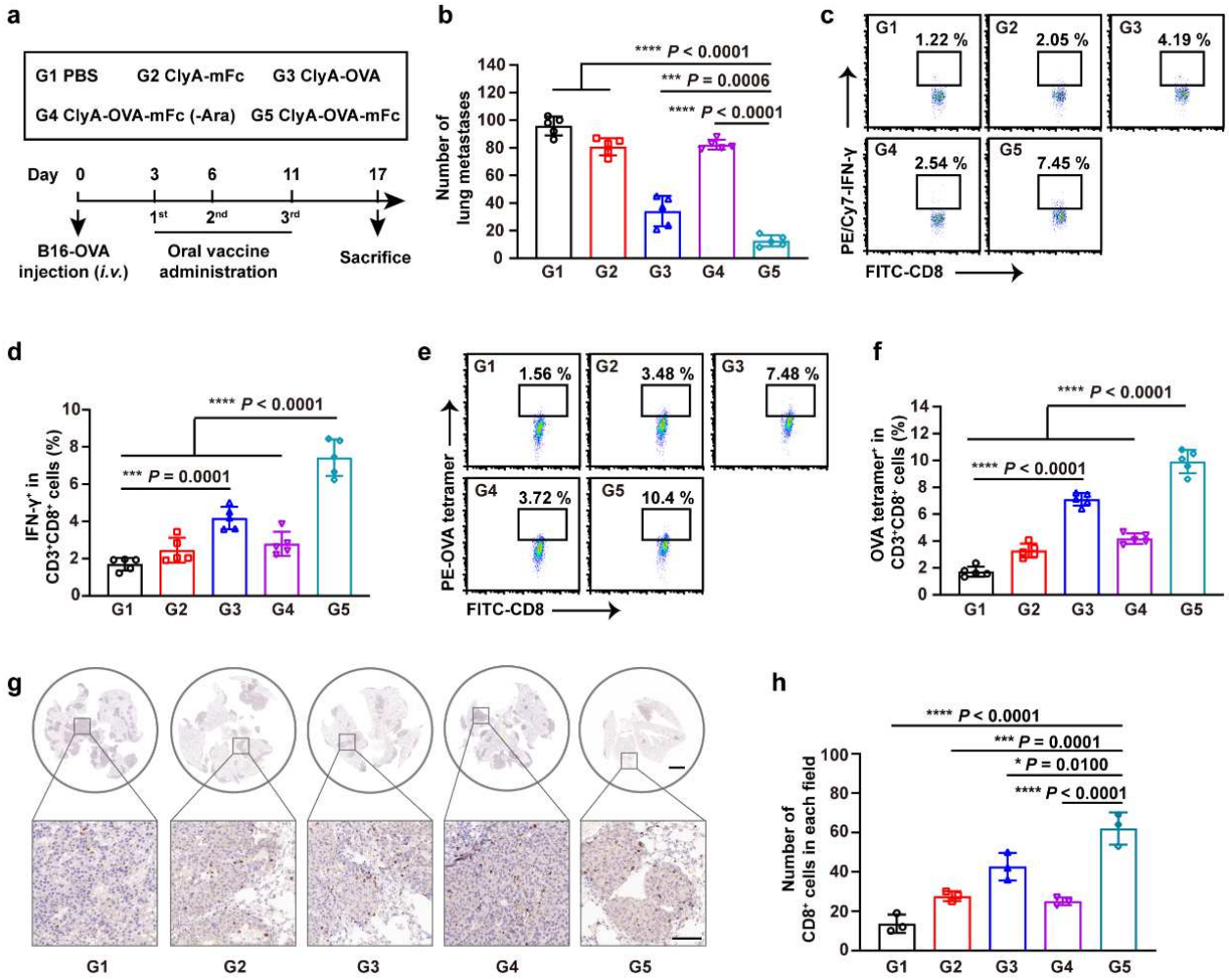

Figure 4 | Evaluation of the antitumor effects of the oral vaccines in a lung metastatic melanoma model. **a,** Schema showing the timeline of model construction and oral vaccination. C57BL/6 mice received an *i.v.* injection of B16-OVA cells on day 0, then were immunized with the indicated oral vaccines on days 3, 6 and 11. Lung metastasis and immune responses were analyzed on day 17. **b,** Quantitative analysis of lung metastasis (n = 5). **c-f,** Antigen-specific immune response analysis. The splenocytes were collected on day 17 and stimulated with OVA peptide. The percentages of IFN-γ$^+$ (**c,d**) or OVA tetramer$^+$ (**e,f**) in CD3$^+$CD8$^+$ cells in the splenocytes were analyzed by flow cytometry (n = 5). **g-h,** Immunohistochemical staining of CD8$^+$ cells (brown staining) in the lung tissues collected on day 17 (**g**) and the quantitation of CD8$^+$ cells in each field (n = 3; **h**). Scale bar, 2 mm in the upper panels and 100 μm in the lower panels. The data are presented as the mean ± SD and were analyzed by one-way analysis of variance (ANOVA) with GraphPad Prism software. N.S., no significance; *, $P < 0.05$; **, $P < 0.01$; ***, $P < 0.001$; ****, $P < 0.0001$.

Antitumor effects in a subcutaneous colon cancer model

A subcutaneous MC38 tumor model was established by subcutaneous injection of MC38 tumor cells on day 0 (**Figure 5a**). We then introduced the specific antigen Adpgk (ASMTNMELM) from MC38 cells into our oral tumor vaccine: ClyA-Adpgk and ClyA-Adpgk-mFc. Mice received 3 treatments (day 3, 6 and 11) of orally administered PBS, ClyA-mFc, ClyA-Adpgk or ClyA-Adpgk-mFc vaccine (**Figure 5a**). In addition, a mixture of adjuvant Poly(I:C) and Adpgk peptide [Poly(I:C) + Adpgk] was injected subcutaneously as a positive control (**Figure 5a**), which formulation strategy is common in clinical trials of tumor vaccines [38,39].

Tumor volumes were recorded every two days until day 19. As shown in **Figure 5b and Supplementary figure 6a**, the mice in the oral ClyA-Adpgk-mFc vaccine group exhibited a stronger inhibition of tumor growth compared to the mice in other groups. The tumors were harvested on day 19 (**Supplementary figure 6b**), and the tumor weight in the oral ClyA-Adpgk-mFc vaccine group was also the lowest compared with that in the other groups (**Figure 5c**). We calculated the tumor inhibition rate according to the tumor volume at the endpoint (**Figure 5d**). Compared with the oral PBS group, the tumor inhibition rate in the oral ClyA-Adpgk-mFc vaccine group was 81.2%, which was higher than the 64.1% in the subcutaneous Poly(I:C) + Adpgk vaccine groups. In addition, we examined the body weight and morphology of the major organs in the different groups (**Supplementary figures 7 and 8**), all of which demonstrate that these oral vaccines were well tolerated, with no apparent toxicity.

We evaluated the antigen-specific immune response in blood and splenocytes, respectively. Increased proportions of Adpgk tetramer$^+$ cells in CD3$^+$CD8$^+$ T cells in blood were found in the oral ClyA-Adpgk-mFc vaccine and subcutaneous Poly(I:C) + Adpgk vaccine groups; this effect was stronger in mice immunized with the oral ClyA-Adpgk-mFc vaccine (**Figure 5e**). The gating strategies and representative flow plots were presented in **Supplementary figures 9a and 9b**. Next, the enzyme-linked immunospot (ELISPOT) assay was used to examine IFN-γ secretion from splenocytes re-stimulated with Adpgk antigen peptide (**Figure 5f**). As expected, most IFN-γ was produced by the splenocytes from the mice immunized with the oral ClyA-Adpgk-mFc vaccine (**Figure 5g**). These results further confirm that our oral vaccine successfully activated the antigen-specific immune response more strongly than the common formulation used in clinical trials.

Next, we detected the infiltrating immune cells in the tumor tissues by flow cytometry. The cells we assessed included CD3$^+$ T cells, CD3$^+$CD4$^+$ T cells, CD3$^+$CD8$^+$ T cells (**Supplementary figures 10a and 10b**), CD11c$^+$ DCs, CD3$^+$CD4$^+$CD25$^+$ regulatory T cells (Tregs; **Supplementary figures 11a and 11b**), CD11b$^+$Ly6G$^+$ activated neutrophils (**Supplementary figures 12a and 12b**), F4/80$^+$ macrophages and CD11b$^+$Gr1$^+$ myeloid-derived suppressor cells (MDSCs; **Supplementary figures 13a and 13b**). Compared with that in the oral PBS group, the tumor-infiltrating CD3$^+$ T cells, CD3$^+$CD8$^+$ T cells, CD3$^+$CD4$^+$ T cells and CD11c$^+$ DCs were significantly elevated in the MC38 tumor tissues from the mice immunized with the oral ClyA-Adpgk-mFc vaccine (**Figure 5h**). The infiltration of these cells induced by oral ClyA-Adpgk-mFc vaccine was greater than the conventional subcutaneous Poly(I:C) + Adpgk vaccine (**Figure 5h**). The tumor-infiltrating CD11b$^+$Ly6G$^+$ activated neutrophils were also increased in the oral ClyA-Adpgk-mFc vaccine group (**Figure 5h**). The immunosuppressive CD3$^+$CD4$^+$CD25$^+$ Tregs in the tumor microenvironment were significantly inhibited by oral vaccination with ClyA-Adpgk-mFc (**Figure 5h**). Similar to the other vaccine groups, there was an infiltration of CD11b$^+$Gr1$^+$ MDSCs in the oral ClyA-Adpgk-mFc vaccine group, although the intratumor infiltration of MDSCs did not interfere with the antitumor effects (**Figure 5h**). Finally, immunofluorescence staining was used to detect CD8$^+$ T cell infiltration in tumor tissues (**Figure 5i**). As expected, the greatest number of infiltrating CD8$^+$ T cells was found in the oral ClyA-Adpgk-mFc vaccine group (**Figure 5j**).

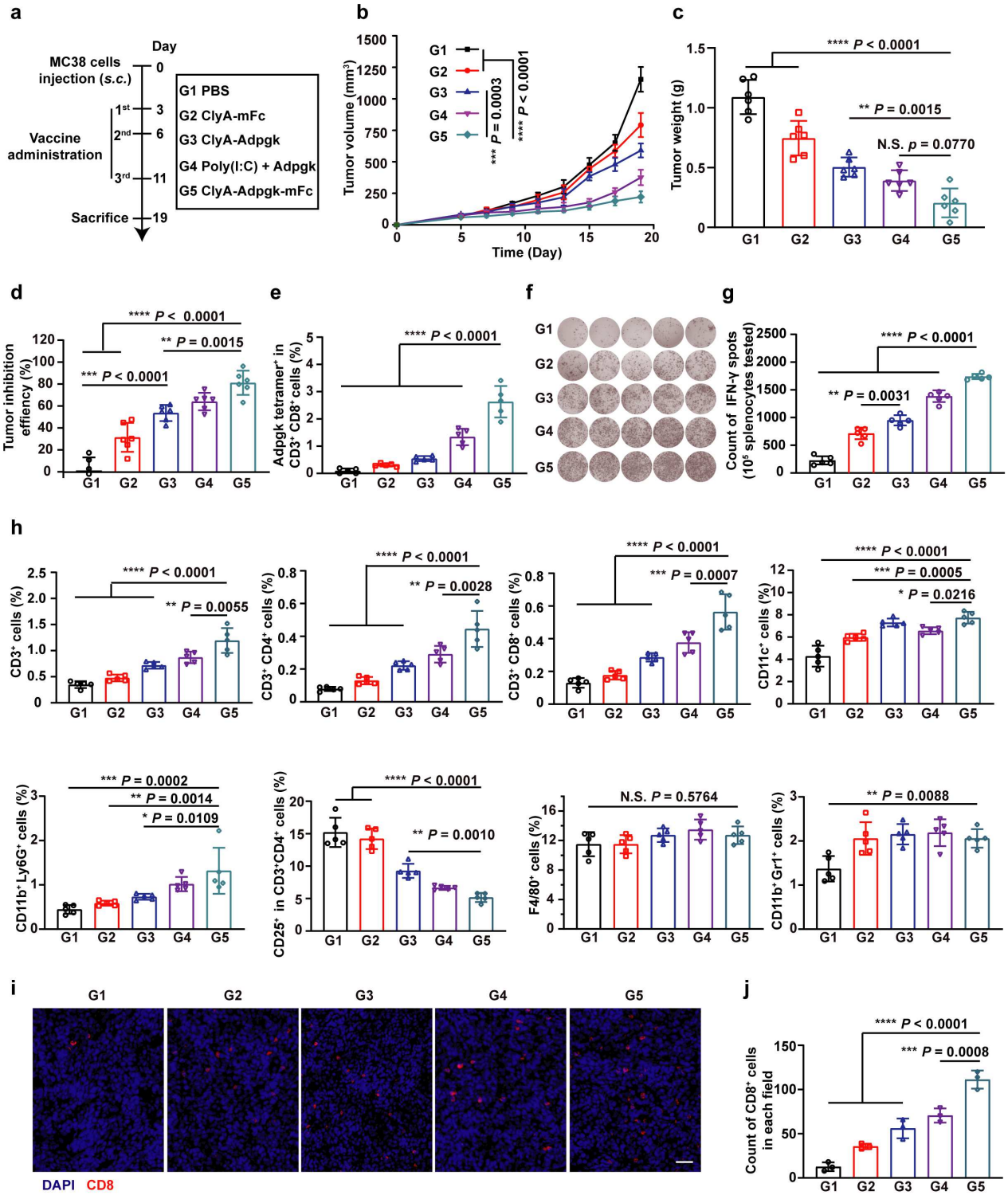

Figure 5 | Evaluation of the antitumor effects of the oral vaccines in a subcutaneous colon cancer model. a, Schema showing the timeline of model construction and oral vaccination. C57BL/6 mice received a *s.c.* injection of MC38 cells on day 0, then were immunized with the indicated oral vaccines on days 3, 6 and 11. A mixture of adjuvant, Poly(I:C), and Adpgk peptide (Poly(I:C) + Adpgk) was injected subcutaneously as a positive control. The mice were sacrificed on day 19, and the tumor tissues, blood and splenocytes were collected. **b,** The tumor volumes were recorded every two days until day 19. **c,** The tumor weight was measured on day 19 (n = 6). **d,** Tumor inhibition rates according to the tumor volumes at the endpoint compared with the oral PBS group (n = 6). **e,** Quantitative analysis of Adpgk tetramer⁺ in $CD3^+CD8^+$ cells in the blood using flow cytometry (n = 5). **f-g,** The IFN-γ secretion by splenocytes after re-stimulation with Adpgk peptide was determined by the ELISPOT assay (**f**) and quantitative analysis (**g**; n = 5). **h,** The infiltrating immune cells in the tumor tissues were detected by flow cytometry, including $CD3^+$ T cells, $CD3^+CD4^+$ T cells, $CD3^+CD8^+$ T

cells, $CD11c^+$ DCs, $CD3^+CD4^+CD25^+$ Tregs, $CD11b^+Ly6G^+$ activated neutrophils, $F4/80^+$ macrophages and $CD11b^+Gr1^+$ MDSCs (n = 5). **i-j,** Immunofluorescence staining of $CD8^+$ cells (red) in the tumor tissues collected on day 19 (**i**) and the quantitation of $CD8^+$ cells in each field (n = 3; **j**). Scale bar, 50 μm. The data are presented as the mean ± SD and were analyzed by one-way analysis of variance (ANOVA) with GraphPad Prism software. N.S., no significance; *, $P < 0.05$; **, $P < 0.01$; ***, $P < 0.001$; ****, $P < 0.0001$.

Evaluation of long-term immune memory

To investigate the long-term immune memory and benefits of treatment with the oral vaccine formulations, we treated healthy mice 3 times with the various oral vaccinations on days 0, 3 and 8 (**Figure 6a**). Splenocytes were isolated on day 50 and the proportions of central memory T cells and effector memory T cells were analyzed by flow cytometry (**Figure 6b and Supplementary figure 14**). As shown in **Figure 6c**, the proportion of effector memory T cells ($CD3^+CD8^+CD44^+CD62L^-$) in the oral ClyA-OVA-mFc vaccine group was significantly greater than that in the other oral vaccine and PBS groups. Although a decrease in central memory T cells ($CD3^+CD8^+CD44^+CD62L^+$) was observed in the oral ClyA-OVA-mFc vaccine group compared with that in the PBS group, similar phenomena were observed in the other oral vaccine groups (**Figure 6d**). Next, the immunized mice were challenged with B16-OVA cells by tail vein injection on day 50, and the lungs were harvested on day 65 and imaged (**Figure 6e**). In contrast to the dense metastases in the PBS, oral ClyA-mFc vaccine and oral ClyA-OVA-mFc (-Ara) vaccine groups, the pulmonary metastases in the oral ClyA-OVA vaccine and oral ClyA-OVA-mFc vaccine groups were significantly reduced, with the protective effect against tumor challenge stronger in the oral ClyA-OVA-mFc vaccine group (**Figure 6f**). Collectively, these results verify that the oral bacteria-derived OMV-based tumor vaccine can induce effective immune memory, which is critical for a long-term prevention of tumor recurrence.

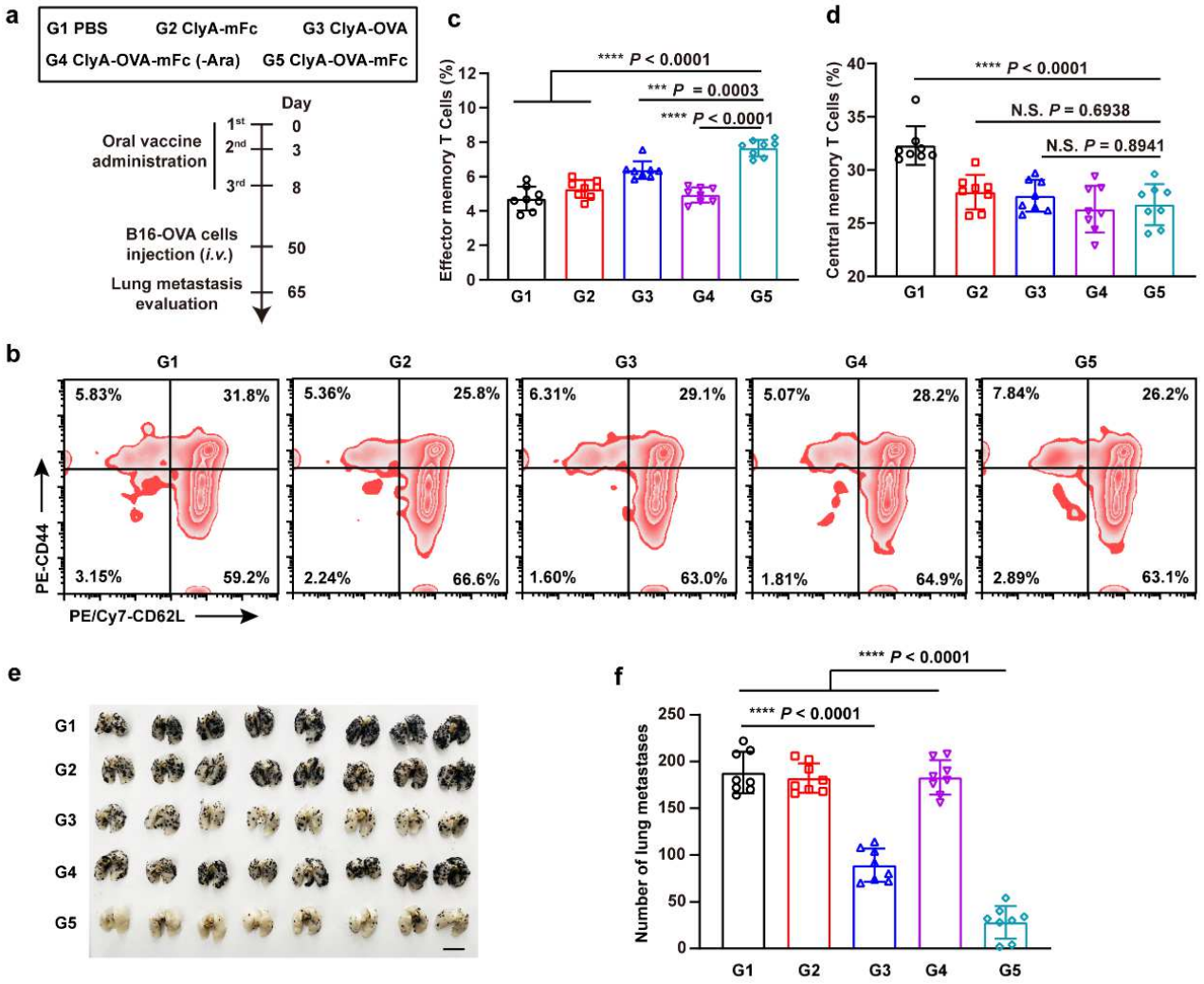

Figure 6 l Evaluation of long-term immune memory elicited by the oral vaccines. a, Schema showing the timeline of model construction and oral vaccination. C57BL/6 mice were immunized with the indicated oral vaccines 3 times on days 0, 3 and 8. The splenocytes were collected for immune memory analysis on day 50. The mice received a tumor challenge of B16-OVA by *i.v.* injection on day 50, and the lungs were excised on day 65 to evaluate the resistance to tumor challenge. **b-d,** Immune memory analysis on day 50. Using flow cytometry (**b**), the proportions of effector memory T cells ($CD3^+CD8^+CD44^+CD62L^-$) (**c**) and central memory T cells ($CD3^+CD8^+CD44^+CD62L^+$) (**d**) in the splenocytes were detected (n = 8). **e-f,** Evaluation of resistance to tumor challenge. The lungs were collected on day 65 (**e**) and the number of tumor nodules were enumerated (**f**; n = 8). Scale bar, 1 cm. The data are presented as the mean ± SD and were analyzed by one-way analysis of variance (ANOVA) with GraphPad Prism software. N.S., no significance; ***, $P < 0.001$; ****, $P < 0.0001$.

Conclusions

Here we present an oral tumor vaccine that differs from previous nanomaterials-based oral vaccine delivery technologies in that it comprises bacteria-membrane vesicle-derived particles [4]. Inspired by the natural phenomenon that commensal bacteria in the gastrointestinal tract can interact with the host immune cells through OMVs, we engineered bacteria to develop an oral tumor vaccine [23]. In some previous studies, engineered bacteria were directly explored for tumor treatment, achieving targeted proliferation and drug delivery to tumor tissue through the complex genetic engineering [40,41]. In the present study, the working environment of the oral vaccine was the intestine, which, as an application strategy, is more biocompatible given the large number of commensal bacteria in the organ. In addition, we exploited bacteria-secreted OMVs

as messengers for tumor antigen delivery. This natural mechanism-mediated epithelial penetration is similar to that in live attenuated virus vaccines, however the non-viral delivery vehicles, OMVs, possess much enhanced biosafety profile. This natural OMV-inspired epithelial penetration strategy may have implications for the development of mucosal vaccines at other sites.

Behavioral controllability is a major challenge for *in vivo* applications of engineered bacteria [42]. Although we found that most of the engineered bacteria were cleared after 24 h, it was still necessary to control the production of OMVs loaded with tumor antigens to avoid immune tolerance due to long-term antigen stimulation. In some previous studies of bacterial applications *in vivo*, a common approach to control gene expression in engineered bacteria has been to introduce an environment-responsive promoter, such as one that responds to hypoxia or low pH in the tumor microenvironment [40,43,44]. However, an environment-responsive promoter is not a bona fide switch type of control method; once the engineered bacteria are exposed to the target environment, the gene expression remains in the open status. Therefore, we adopted an arabinose-inducible promoter to achieve switchable control of the engineered bacteria through inducer administration [45] .

In summary, we genetically engineered *E. coli*, one of the most abundant commensal bacteria in the gut, to establish a bacteria-derived OMV-based oral tumor vaccine. Using this strategy, we achieved *in situ* controllable production of OMVs loaded with tumor antigen in the intestine. Together with the tumor antigen, OMVs effectively crossed the intestinal epithelial barriers to be recognized by immune cells in the lamina propria, thus efficiently activating a tumor antigen-specific immune response, leading to significant inhibition of tumor growth. This strategy possesses enormous potential for the development of orally tumor vaccines.

Methods

Materials. Dulbecco's Modified Eagle Medium (DMEM; 319-005-CL) and fetal bovine serum (FBS; 085-150) were obtained from Wisent Bio Products (St. Bruno, Canada); Arabinose (A106196-100 g) was purchased from Aladdin Biochemical Technology Co., Ltd. (Shanghai, China); Radio immunoprecipitation assay (RIPA) lysis buffer (R0010) and percoll were purchased from Solarbio Life Science (Beijing, China); DAPI was obtained from Life Technologies (Shanghai, China); D-Luciferin (D1007) was purchased from US EVERBRIGHT Inc. (Suzhou, China); Cell dishes and 96-well culture plates were obtained from Hangzhou Xinyou Biotechnology Co., Ltd. (Hangzhou, China); Ampicillin (T0814L-200 mg) was obtained from Target Molecule Corp (TargetMol, USA); anti-HA-Tag (100028-MM15-50) was purchased from Sino Biogical Inc. (Beijing, China); FITC-anti-mouse CD3 (100204), PE-anti-mouse CD4 (100408), APC-anti-mouse CD8α (100712), PE/Cy7-anti-mouse IFN-γ (505826), FITC-anti-mouse CD11c (117306), PE/Cy7-anti-mouse CD80 (104734), APC-anti-mouse CD86 (105012), PE/Cy7-anti-mouse F4/80 (123114), PE-anti-mouse CD11b (101208), FITC-anti-mouse Ly6G (127606), PE-anti-mouse CD44 (103008) and PE/Cy7-anti-mouse CD62L (104418) antibodies for flow cytometry analysis were purchased from BioLegend Inc. (San Diego, USA). T-Select H-2Kb OVA Tetramer-SIINFEKL-PE (TS-5001-1C) and T-Select H-2Db Adpgk Tetramer-ASMTNMELM-PE (TB-5113-1) were purchased from MBL Beijing Biotech Co., Ltd. The mouse IFN-γ

precoated ELISPOT kit (2210005) was obtained from Dakewe Biotech Company Ltd. (Shenzhen, China). $OVA_{257-264}$ (SIINFEKL), Adpgk (CGIPVHLELASMTNMELMSSIVHQQVFPT) were synthesized by Top Peptide (Shanghai, China).

Animal and cells. Female C57BL/6 (6-8 weeks old) were obtained from SPF Biotechnology Co., Ltd. (Beijing, China). All animal experiments were approved by the Ethics Committee of the National Center for Nanoscience and Technology of China. The murine melanoma cell B16-F10 and B16-OVA cells were cultured in DMEM containing 10% FBS, 100 U/mL penicillin G sodium, 100 μg/mL streptomycin at 37℃ in a humidified environment with 5% CO_2.

Plasmid construction and genetically engineered bacteria growth. The Luc-HA gene was cloned into the pBAD vector (Genewiz, Suzhou, China) at the NcoI and EcoRI restriction sites. The ClyA-mFc, ClyA-OVA, ClyA-OVA-mFc, ClyA-Adpgk and ClyA-Adpgk-mFc were cloned into the pBAD vector (Genewiz, Suzhou, China) at the EcoRI and HindIII restriction sites. The *E. coli* strain Top10, which had been transformed with the expression plasmids, pBAD-ClyA-mFc, pBAD-ClyA-OVA, pBAD-ClyA-OVA-mFc, pBAD-ClyA-Adpgk or pBAD-ClyA-Adpgk-mFc, was grown at 37℃ in LB medium with shaking at 180 rpm. Ampicillin (60 μg/mL) was added when needed.

***In vitro* and *in vivo* bioluminescence assay.** *E. coli* transformed with luciferase-HA plasmids and control *E. coli* were cultured with or without 2 g/L arabinose solution. 10^8 engineered *E. coli* were suspended in PBS and 50 μL 15 mg/mL D-Luciferin potassium solution was added. Female C57BL6 were administered 10^8 *E. coli* and treated with drinking water containing 10 g/L arabinose. After 12 h, the mice were sacrificed and 20 mg of the contents from the stomach, intestine, cecum and colon and feces were collected into 1.5 mL tubes and suspended in 300 μL 15 mg/mL D-Luciferin potassium solution. The samples were assessed by measuring the bioluminescence using an IVIS system and Living Image Software.

Ara dose screening assay. To determine the effect of arabinose dosage on expression of the system, female C57BL6 were orally administered engineered *E. coli* on the first day and treated with four different concentrations of arabinose water for 12 h. 20 mg feces were collected into 1.5 mL tubes and suspended in 300 μL 15 mg/mL D-Luciferin potassium solution for bioluminescence detection.

Pharmacokinetic study. Female C57BL6 mice were orally administered 10^9 engineered *E. coli* and 20 g/L arabinose water. The mice were then euthanized at 0, 2, 5, 12 and 24 h and the digestive tract tissue (from stomach to colon) were isolated. 2 mL 15 mg/mL D-Luciferin potassium solution was infused into the digestive tract for bioluminescence analysis.

OMVs preparation and characterization. TOP10 bacteria were cultured as described above and arabinose (2 g/L) was added to further induce protein expression when the OD_{600} reached 0.6-0.8. Bacteria was incubated overnight at 16℃ with shaking at 160 rpm and removed by centrifugation at 5000 ×*g* for 10 min at 4℃. The supernatant (200 mL) was filtered through a 0.45 μm polyvinylidene fluoride filter (Millipore, R8SA47939, USA) and concentrated to 50 mL using a 50 kDa ultrafiltration membranes (Millipore, R3EA06699, USA). The concentrated solution was again filtered with a 0.22 μm filter (Millipore, R9HA36284,

USA). OMVs were collected by ultracentrifugation at 150,000 ×*g* for 3 h at 4℃. The pellet was finally resuspended in 200 μL PBS and passed through a 0.22 μm filter to remove intact bacteria or cell debris. The filtrate was stored at -20℃ until further use. The morphology of OMVs was characterized by transmission electron microscopy (TEM; HT7700 electron microscope; Hitachi, Japan) and the size of OMVs was measured using dynamic light-scattering (DLS; Zetasizer Nano AS90, Malvern, UK).

.

Western blot Analysis. Heterologous protein expression in engineered bacteria and OMVs was analyzed by western blot analysis. For engineered bacteria, the total protein was extracted using a Bacterial Protein Extraction Kit (Beijing Puyihua Science and Technology Co., Ltd., China, catalog No. C600596) according to the manufacturer's instructions. To extract the protein of OMVs, the vesicles were lysed for 15 min using RIPA buffer containing 1 mM PMSF. The lysis solution was centrifugated at 12,000 ×*g* for 30 min at 4℃ and the supernatant was collected. The protein concentration of the samples was quantified using a bicinchoninic acid assay (BCA protein assay kit; Thermo Scientific, USA) according to the manufacturer's instructions. Protein lysates (30 μg/sample) were resolved by SDS-PAGE and transferred to a polyvinylidene fluoride (PVDF) membrane. After blocking in 10% non-fat milk, the PVDF membrane was incubated with an anti-HA-tag (1:2,000) and HRP conjugated goat anti-rabbit IgG (1:10,000). Immunoreactive proteins were visualized using enhanced chemiluminescence reagents (Bio-Rad, USA).

Evaluation of intestinal epithelium penetration of OMVs. After 6 h of fasting, mice were anesthetized, and the colon was ligated with sutures (about 2 cm in length). 50 μg Control OMVs, ClyA-HA-mFc OMVs, ClyA-HA-OVA OMVs or ClyA-HA-OVA-mFc OMVs were injected into the ligated intestinal cavity and incubated for 2 h. An animal body temperature device was used to ensure a constant body temperature during the experiment.

Immune stimulation by oral vaccine *in vivo.* Female C57BL6 mice orally received ClyA-HA-mFc, ClyA-HA-OVA or ClyA-HA-OVA-mFc engineered bacteria or PBS and were treated with or without 20 g/L arabinose water for 12 h (n = 4). Mice were euthanized after 24 h of vaccination and the lamina propria lymphocytes (LPLs) in the intestine were isolated and DC maturation was analyzed using flow cytometry. For investigation of specific immune responses, the mice received the different oral vaccine formulations at day 0, 3 and 8. Splenocytes were harvested on day 12 for further flow cytometer analysis (n = 4). In order to analyze specific tumor killing, the mice were treated as above and the splenocytes collected from different groups were incubated with B16-OVA cells or MC38 cells for 24 h (n = 8). The cell viability was measured using a CCK-8 kit according to the manufacturer's protocols.

Isolation of LPLs in the intestine. LPLs were isolated as previously described with slight modification [46]. Briefly, the colon tissue of mice was collected and placed in ice-cold PBS. The feces, residual mesenteric fat tissue and Peyer's patches (PPs) were removed. The intestine was then opened longitudinally and cut into 1 cm pieces for further usage. The pieces of intestine were incubated in 5 mL pre-digestion solution (5 mM EDTA, 1 mM Sigma-Aldrich in Ca^{2+}, Mg^{2+}-free Hank's balanced salt solution) for 20 min at 37℃ under shaking (200 rpm). The solution was vortexed for 30 seconds and passed through a 70 μm cell strainer. The remaining pieces of intestine were treated as above and then transferred into a new 50 mL tube with 5 mL digestion

solution (RPMI 1640 containing 1.5% FBS, 0.5 mg/mL collagenase IV, 0.5 mg/mL collagenase I and 0.04mg/mL DNase I). The solution was incubated at 37℃ for 1 h (shaken at 200 rpm) and vortexed for 30 seconds before passing through a 70 μm cell strainer. The remaining pieces were collected and placed in fresh digestion solution. The above digestion protocols were repeated again and the filtered digestion solution was collected. The filtrate was centrifugated at 500 ×*g* for 20 min and the sediment containing the LPLs was collected for flow cytometry analysis.

Immunization and antitumor efficacy in lung metastasis models. To evaluate the tumor therapeutic effects of the oral vaccines in lung metastasis models, C57BL/6 mice were injected intravenously with murine B16-OVA melanoma cells (2×10^5 cells) on day 0. The mice were orally administered ClyA-HA-mFc, ClyA-HA-OVA or ClyA-HA-OVA-mFc engineered bacteria (10^9 cells/mouse) on days 3, 6 and 11, and were provided 20 g/L arabinose solution for 12 h to induce protein expression after each vaccination. Mice administered PBS were used as the control group. On day 17, the mice were euthanized (n = 5) and the spleens and lungs were collected for further analysis. The lungs were washed with PBS and fixed using Fekete's buffer (volume ratio, 75% alcohol: formalin: glacial acetic acid = 14: 2: 1) for 48 h. The number of pulmonary tumor metastases was counted.

To analyze the intracellular IFN-γ and OVA tetramer positive T cells in the spleen, splenocytes collected at the end of the experiment were incubated with OVA peptide overnight to re-stimulate the T lymphocytes. Splenocytes treated with ionomycin were used as a positive control group. For intracellular IFN-γ staining, the surface proteins CD3 and CD8 were first stained before fixation of the cells with a commercially available fixation buffer (BioLegend, USA, Catalog No. 420801). After fixation and permeabilization, the cells were subjected to IFN-γ staining. Finally, the cells were washed with PBS and analyzed using a flow cytometer. For OVA tetramer positive T cell staining, T-Select MHC Tetramer was added prior to the CD3 and CD8 flow cytometry antibodies. After incubation with T-Select MHC Tetramer for 30 min at 4℃, the cells were stained with CD3 and CD8 antibodies for another 30 min and analyzed using a flow cytometer.

Immunohistochemical analysis of T lymphocyte infiltration into lungs. The lungs harvested at the end of the lung metastasis experiment were fixed with 4% paraformaldehyde and embedded in paraffin, which was cut into 7 μm sections for immunohistochemical staining of CD8. The sections were deparaffinized, rehydrated and treated with 3% H_2O_2 to eliminate the activity of endogenous peroxidase. The sections were subjected to antigen retrieval, blocking with 5% goat serum and incubation with an anti-CD8 antibody (Abcam, UK, catalog No. ab93278, dilution: 1:100) overnight. The sections were then incubated sequentially with a goat anti-rabbit IgG biotinylated antibody (Biorbyt, UK, catalog No. orb153693, dilution: 1:100) and HRP-conjugated streptavidin. Finally, the sections were stained with DAB for color development and counterstained with hematoxylin.

Antitumor efficacy in subcutaneous colon tumor models. In order to evaluate the antitumor effect of the oral vaccines in a solid tumor model, 2×10^6 murine colon adenocarcinoma (MC38) cells were injected subcutaneously into the right flank of C57BL/6 mice on day 0. The mice were orally administered with ClyA-HA-mFc, ClyA-HA-Adpgk or ClyA-HA-Adpgk-mFc engineered bacteria or PBS on days 3, 6 and 11 (n = 6).

Mice were provided 20 g/L arabinose water for 12 h after each vaccination, if applicable. Mice subcutaneously immunized with a mixture of 50 μg adjuvant Poly (I:C) + 50 μg Adpgk were used as a positive control group. Mice treated with PBS were used as a negative control group. The tumor volume was measured every other day using Vernier calipers and calculated by the following formula: tumor volume = length × 1/2 width^2. The mice were euthanized on day 19. The tumors were harvested, weighed and digested into single cell suspensions to analyze the infiltrating immune cells by flow cytometry and immunofluorescence. Spleens were collected for IFN-γ ELISPOT analysis. According to the manufacturer's instructions, splenocytes were seeded in a 96-well plate (1 × 10^5 cells/well), pre-coated with a mouse anti-IFN-γ antibody, and incubated with Adpgk peptide or ionomycin for 20 h. A biotinylated antibody specific for IFN-γ and alkaline-phosphatase conjugated to streptavidin were subsequently used to detect the IFN-γ secreted by the restimulated T cells. By adding a substrate solution, visual spots were formed at the sites of captured IFN-γ, and automated spot quantification was caried out by Dakewe Biotech Co., Ltd. The major organs, including heart, liver, spleen, lung and kidney, were collected for hematoxylin and eosin (H&E) staining.

Long-term immune memory. C57BL/6 mice (6-8 weeks, female) were administered oral vaccination or PBS on days 0, 3 and 8. To analyze memory T cells, splenocytes were collected at day 50 (n = 8) and labelled with anti-CD3, anti-CD8, anti-CD44 and anti-CD62L antibodies. The central memory T cells ($CD3^+CD8^+CD44^+CD62L^+$) and effector memory T cells ($CD3^+CD8^+CD44^+CD62L^-$) were analyzed by flow cytometry. To investigate the effects of prophylactic tumor challenge, the vaccinated mice (n = 8) were intravenously injected with B16-OVA cells (2 × 10^5) on day 50 and euthanized on day 65. The lungs were harvested, fixed and photographed. The number of pulmonary tumor nodes was counted.

Immunofluorescence. Samples were collected and rapidly frozen in optimal cutting temperature (OCT) compound. They were then cut into sections (7 μm) and washed with PBS three times to remove OCT compound. The sections were incubated with 0.1% Triton X-100 for 30 min, blocked using 10% goat serum for 1 h and incubated overnight with an anti-CD11b antibody (GB11058, Servicebio, China), anti-HA-tag antibody (ab1424, Abcam, USA) or anti-CD8 antibody (ab203035, Abcam, USA), followed by washing three times with PBS and incubating with secondary antibodies conjugated with Alexa Fluor 488 for 2 h. Nuclei were stained with DAPI. The sections were analyzed using a confocal microscope (Zeiss LSM710, Germany).

Statistical analysis. The data are presented as means ± SD. One-way analysis of variance (ANOVA) was used for multiple comparisons. GraphPad Prism 5 and FlowJo V10 were used to analyze experimental data. Statistical significance was set as follows: $^*P < 0.05$, $^{**}P < 0.01$, $^{***}P < 0.001$, $^{****}P < 0.0001$, and N.S. denotes no significant difference.

Data availability

Source data are provided with this paper or available from the corresponding author upon reasonable request.

References

1. Kirkwood, J. M. *et al.* Immunotherapy of cancer in 2012. *CA. Cancer J. Clin.* **62**, 309-335 (2012).

2. Sahin, U. & Türeci, Ö. Personalized vaccines for cancer immunotherapy. *Science* **359**, 1355-1360 (2018).
3. Mathias Vormehr, Ö. T., & Sahin, U. Harnessing Tumor Mutations for Truly Individualized Cancer Vaccines. *Annu. Rev. Med.* **70**, 395-407 (2019).
4. Vela Ramirez, J. E., Sharpe, L. A. & Peppas, N. A. Current state and challenges in developing oral vaccines. *Adv. Drug. Deliv. Rev.* **114**, 116-131 (2017).
5. Qin, H. *et al.* Development of a Cancer Vaccine Using In Vivo Click-Chemistry-Mediated Active Lymph Node Accumulation for Improved Immunotherapy. *Adv. Mater.* **33**, e2006007 (2021).
6. Vighi, G., Marcucci, F., Sensi, L., Di Cara, G. & Frati, F. Allergy and the gastrointestinal system. *Clin. Exp. Immunol.* **153 Suppl 1**, 3-6 (2008).
7. Zimmermann, P. & Curtis, N. The influence of the intestinal microbiome on vaccine responses. *Vaccine* **36**, 4433-4439 (2018).
8. Taddio, A. *et al.* Survey of the prevalence of immunization non-compliance due to needle fears in children and adults. *Vaccine* **30**, 4807-4812 (2012).
9. Kim, S. H. & Jang, Y. S. The development of mucosal vaccines for both mucosal and systemic immune induction and the roles played by adjuvants. *Clin. Exp. Vaccine Res.* **6**, 15-21 (2017).
10. New, R. R. C. Formulation technologies for oral vaccines. *Clin. Exp. Immunol.* **198**, 153-169 (2019).
11. Borges, O. *et al.* Evaluation of the immune response following a short oral vaccination schedule with hepatitis B antigen encapsulated into alginate-coated chitosan nanoparticles. *Eur. J. Pharm. Sci.* **32**, 278-290 (2007).
12. Mann, J. F. *et al.* Lipid vesicle size of an oral influenza vaccine delivery vehicle influences the Th1/Th2 bias in the immune response and protection against infection. *Vaccine* **27**, 3643-3649 (2009).
13. Peek, L. J., Middaugh, C. R. & Berkland, C. Nanotechnology in vaccine delivery. *Adv. Drug. Deliv. Rev.* **60**, 915-928 (2008).
14. Wang, J., Li, Y. & Nie, G. Multifunctional biomolecule nanostructures for cancer therapy. *Nat. Rev. Mater.*, 1-18 (2021).
15. Din, M. O. *et al.* Synchronized cycles of bacterial lysis for in vivo delivery. *Nature* **536**, 81-85 (2016).
16. Riglar, D. T. & Silver, P. A. Engineering bacteria for diagnostic and therapeutic applications. *Nat. Rev. Microbiol.* **16**, 214-225 (2018).
17. Zhou, S., Gravekamp, C., Bermudes, D. & Liu, K. Tumour-targeting bacteria engineered to fight cancer. *Nat. Rev. Cancer* **18**, 727-743 (2018).
18. Duan, F. & March, J. C. Engineered bacterial communication prevents Vibrio cholerae virulence in an infant mouse model. *Proc. Natl. Acad. Sci. USA* **107**, 11260-11264 (2010).
19. Hwang, I. Y. *et al.* Reprogramming microbes to be pathogen-seeking killers. *ACS Synth. Biol.* **3**, 228-237 (2014).
20. Yang, C. *et al.* Upconversion optogenetic micro-nanosystem optically controls the secretion of light-responsive bacteria for systemic immunity regulation. *Commun. Biol.* **3**, 561 (2020).
21. Zheng, D. W. *et al.* Prebiotics-Encapsulated Probiotic Spores Regulate Gut Microbiota and Suppress Colon Cancer. *Adv. Mater.* **32**, e2004529 (2020).
22. Ho, C. L. *et al.* Engineered commensal microbes for diet-mediated colorectal-cancer chemoprevention. *Nat. Biomed. Eng.* **2**, 27-37 (2018).

23. Shen, Y. *et al.* Outer membrane vesicles of a human commensal mediate immune regulation and disease protection. *Cell Host. Microbe.* **12**, 509-520 (2012).
24. Chu, H. *et al.* Gene-microbiota interactions contribute to the pathogenesis of inflammatory bowel disease. *Science* **352**, 1116-1120 (2016).
25. Schwechheimer, C. & Kuehn, M. J. Outer-membrane vesicles from Gram-negative bacteria: biogenesis and functions. *Nat. Rev. Microbiol.* **13**, 605-619 (2015).
26. Cheng, K. *et al.* Bioengineered bacteria-derived outer membrane vesicles as a versatile antigen display platform for tumor vaccination via Plug-and-Display technology. *Nat. Commun.* **12**, 2041 (2021).
27. Li, Y. *et al.* Bacterial Outer Membrane Vesicles Presenting Programmed Death 1 for Improved Cancer Immunotherapy via Immune Activation and Checkpoint Inhibition. *ACS Nano.* in press (2021).
28. Kaparakis-Liaskos, M. & Ferrero, R. L. Immune modulation by bacterial outer membrane vesicles. *Nat. Rev. Immunol.* **15**, 375-387 (2015).
29. Stentz, R., Carvalho, A. L., Jones, E. J. & Carding, S. R. Fantastic voyage: the journey of intestinal microbiota-derived microvesicles through the body. *Biochem. Soc. Trans.* **46**, 1021-1027 (2018).
30. Akilesh, S., Christianson, G. J., Roopenian, D. C. & Shaw, A. S. Neonatal FcR expression in bone marrow-derived cells functions to protect serum IgG from catabolism. *J. Immunol.* **179**, 4580-4588 (2007).
31. Sockolosky, J. T. & Szoka, F. C. The neonatal Fc receptor, FcRn, as a target for drug delivery and therapy. *Adv. Drug. Deliv. Rev.* **91**, 109-124 (2015).
32. Baker, K. *et al.* Neonatal Fc receptor expression in dendritic cells mediates protective immunity against colorectal cancer. *Immunity* **39**, 1095-1107 (2013).
33. Nguyen, V. H. *et al.* Genetically engineered Salmonella typhimurium as an imageable therapeutic probe for cancer. *Cancer Res.* **70**, 18-23 (2010).
34. Zheng, J. H. *et al*. Two-step enhanced cancer immunotherapy with engineered Salmonella typhimurium secreting heterologous flagellin. *Sci. Transl. Med.* **9**, 9537-9637 (2017).
35. Hilgendorf, C. *et al.* Caco-2 versus Caco-2/HT29-MTX co-cultured cell lines: permeabilities via diffusion, inside- and outside-directed carrier-mediated transport. *J. Pharm. Sci.* **89**, 63-75 (2000).
36. Li, Y. *et al.* Gut microbiota dependent anti-tumor immunity restricts melanoma growth in Rnf5(-/-) mice. *Nat. Commun.* **10**, 1492 (2019).
37. Chen, Q. *et al.* A Hybrid Eukaryotic-Prokaryotic Nanoplatform with Photothermal Modality for Enhanced Antitumor Vaccination. *Adv. Mater.* **32**, e1908185 (2020).
38. Ott, P. A. *et al.* An immunogenic personal neoantigen vaccine for patients with melanoma. *Nature* **547**, 217-221 (2017).
39. Hu, Z. *et al*. Personal neoantigen vaccines induce persistent memory T cell responses and epitope spreading in patients with melanoma. *Nat. Med.* **27**, 515-525 (2021).
40. Flentie, K. *et al.* A bioluminescent transposon reporter-trap identifies tumor-specific microenvironment-induced promoters in Salmonella for conditional bacterial-based tumor therapy. *Cancer Discov.* **2**, 624-637 (2012).
41. Duong, M. T., Qin, Y., You, S. H. & Min, J. J. Bacteria-cancer interactions: bacteria-based cancer therapy. *Exp. Mol. Med.* **51**, 1-15 (2019).
42. Forbes, N. S. Engineering the perfect (bacterial) cancer therapy. *Nat. Rev. Cancer* **10**, 785-794 (2010).

43. Ryan, R. M. *et al.* Bacterial delivery of a novel cytolysin to hypoxic areas of solid tumors. *Gene Ther.* **16**, 329-339 (2009).
44. Chien, T., Doshi, A. & Danino, T. Advances in bacterial cancer therapies using synthetic biology. *Curr. Opin. Syst. Biol.* **5**, 1-8 (2017).
45. Hong, H. *et al.* Targeted deletion of the ara operon of Salmonella typhimurium enhances L-arabinose accumulation and drives PBAD-promoted expression of anti-cancer toxins and imaging agents. *Cell Cycle* **13**, 3112-3120 (2014).
46. Weigmann, B. *et al.* Isolation and subsequent analysis of murine lamina propria mononuclear cells from colonic tissue. *Nat. Protoc.* **2**, 2307-2311 (2007).

Acknowledgements
This work was supported by grants from the National Key R&D Program of China (2018YFA0208900 and 2018YFE0205300), the Strategic Priority Research Program of the Chinese Academy of Sciences (XDB36000000), the Beijing Natural Science Foundation of China (Z200020), the Beijing Nova Program (Z201100006820031), the National Natural Science Foundation of China (31800838, 31820103004, 31730032 and 51861145302), the Key Research Project of Frontier Science of the Chinese Academy of Sciences (QYZDJ-SSW-SLH022), the Innovation Research Group of the National Natural Science Foundation (11621505) and the Hundred-Talent Program of the Chinese Academy of Sciences.

Author contributions
Y. Y., J. X. and Y. L. contributed equally to this work. Y. Y., J. X., Y. L., X. Z. and G. N. designed the research. Y. Y., J. X., Y. L., K. C., Q. F., X. M., N. M., T. Z. and X. W. performed the research. All authors analyzed and interpreted the data. Y. Y., J. X., Y. L. X. Z. and G. N. wrote the paper.

Competing interests
G.N., X.Z., Y.L. are inventors on a filed provisional application China patent (Oral vaccine system based on membrane vesicle strategy) submitted by the National Center for Nanoscience and Technology that covers the potential diagnostic and therapeutic uses of the oral vaccine for cancer immunotherapy. The authors declare that they have no other competing interests.

Supplementary Information

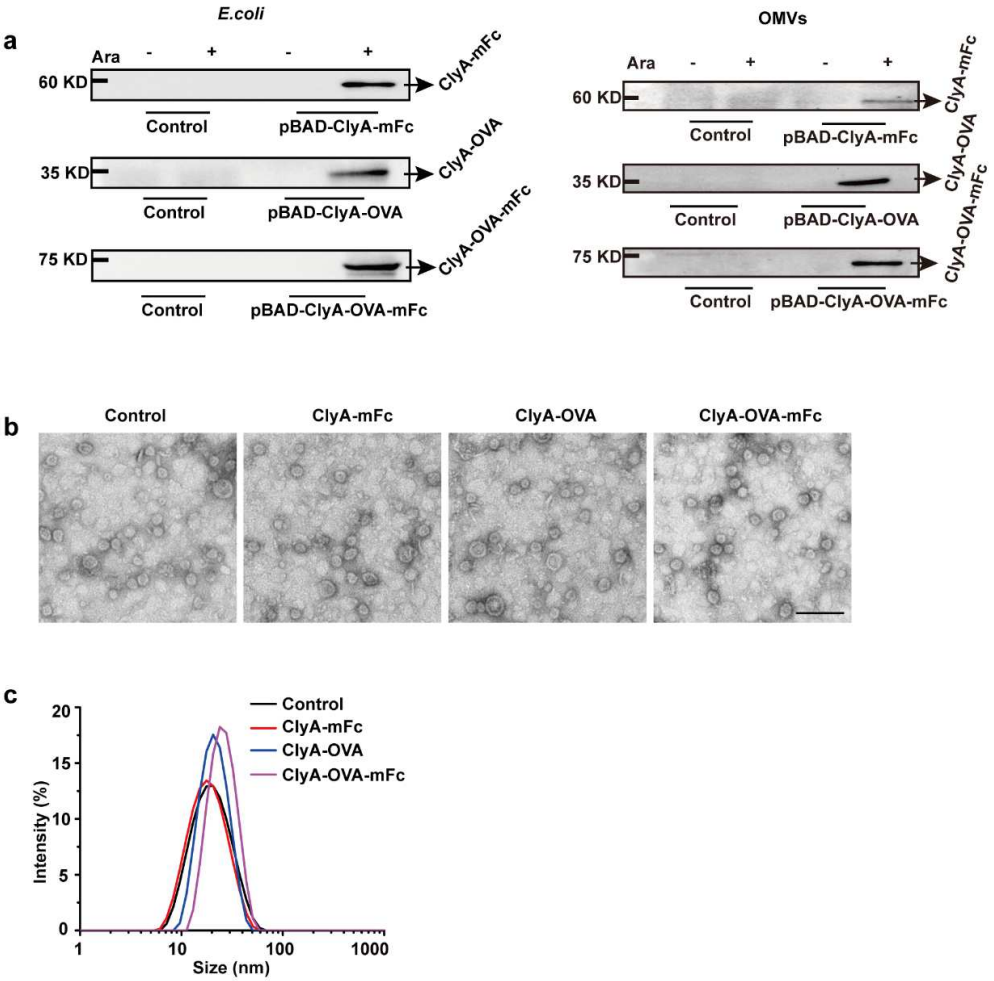

Supplementary figure 1 l Characterization of OMVs from different engineered bacteria. **a,** Western blot analysis of ClyA-mFc, ClyA-OVA and ClyA-OVA-mFc expression in the respective, engineered *E. coli* and their secreted OMVs. Ara was used as the expression inducer. **b,** Morphology of OMVs as analyzed by TEM. Scale bar, 100 nm. **c,** Hydrodynamic size of OMVs detected by DLS.

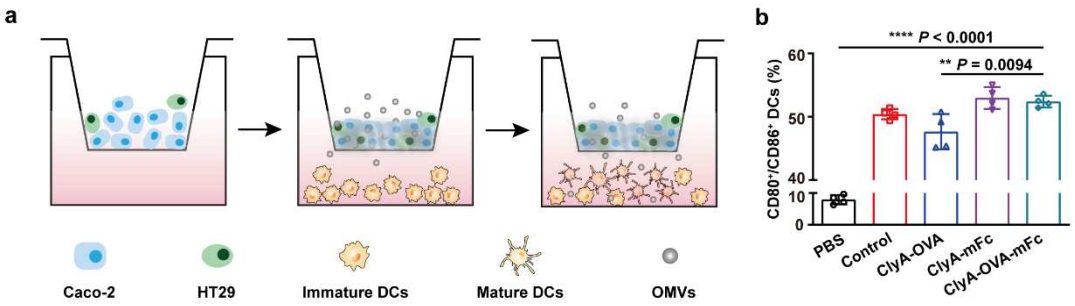

Supplementary figure 2 l Epithelial penetration analysis of OMVs from different engineered bacteria *in vitro*. **a,** Schematic illustration of the transwell system experiment. The Caco-2 cells and HT29 cells were co-cultured in the upper chamber at a ratio of 9:1 for 21 days. Next, DC2.4 cells were seeded in the lower chamber and OMVs from the indicated engineered bacteria were added into the upper chamber. **b,** The percentage of

$CD80^+/CD86^+$ DCs in the lower chamber were analyzed by flow cytometry after 12 h (n = 4). The data are presented as the mean ± SD and were analyzed by one-way analysis of variance (ANOVA) with GraphPad Prism software. *, $P < 0.05$.

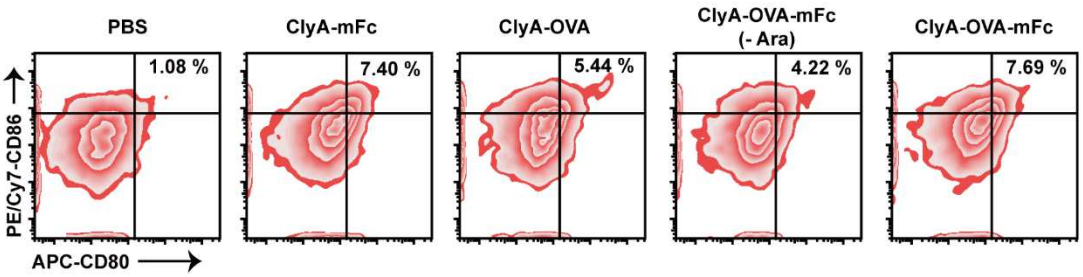

Supplementary figure 3 I Representative images of $CD80^+CD86^+$ in $CD11c^+$ cells measured by flow cytometry in the immune response analysis of immune cells in the lamina propria (cf. Figure 3c).

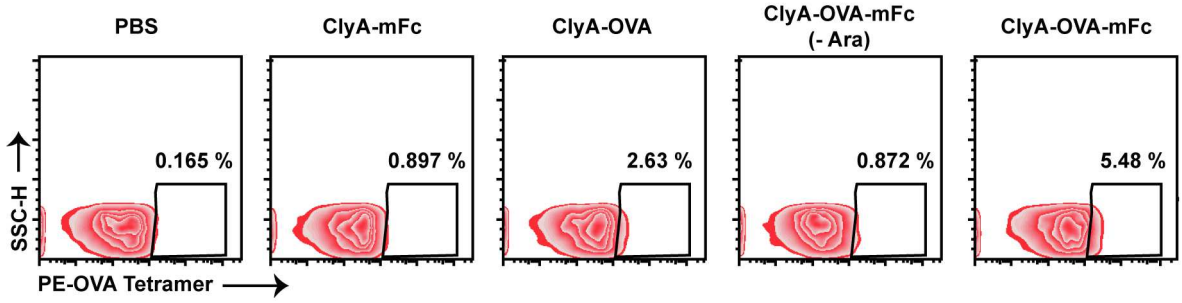

Supplementary figure 4 I Representative images of OVA $tetramer^+$ in $CD3^+CD8^+$ cells measured by flow cytometry in the immune response analysis of splenocytes (cf. Figure 3d).

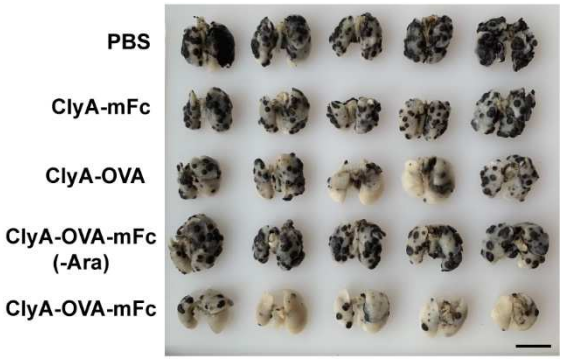

Supplementary figure 5 I Images of lungs dissected from mice in the experiments in the lung metastatic melanoma model. Scale bar, 1 cm.

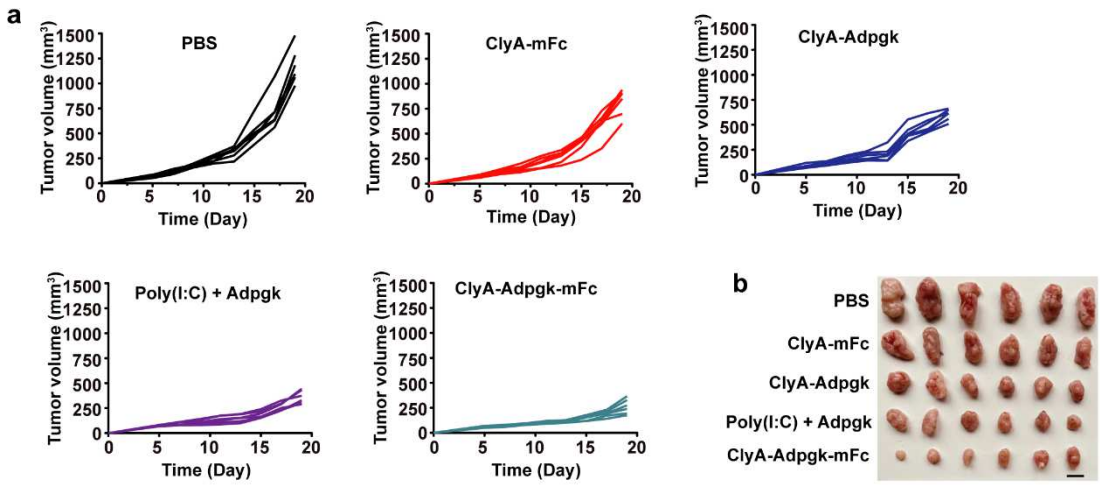

Supplementary figure 6 l The antitumor effects of the oral vaccine in the subcutaneous MC38 tumor model. **a,** Individual tumor growth curves of mice in the indicated groups (cf. Figure 5b). **b,** Image of tumors harvested from mice on day 19 (cf. Figure 5c). Scale bar, 1 cm.

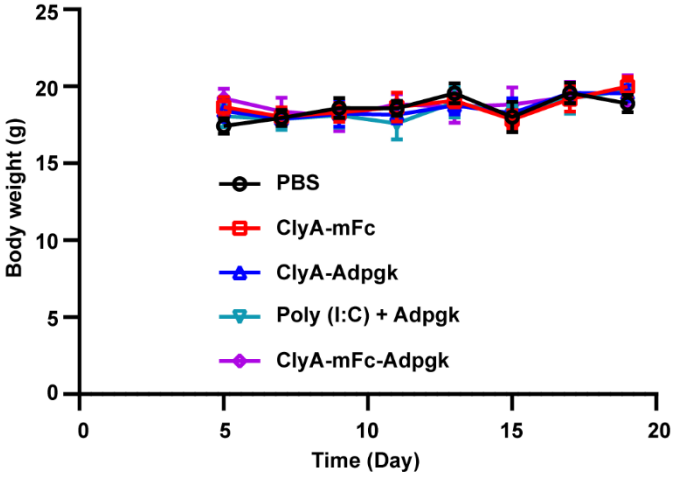

Supplementary figure 7 l Body weights of mice in the subcutaneous MC38 tumor model experiments (n = 6).

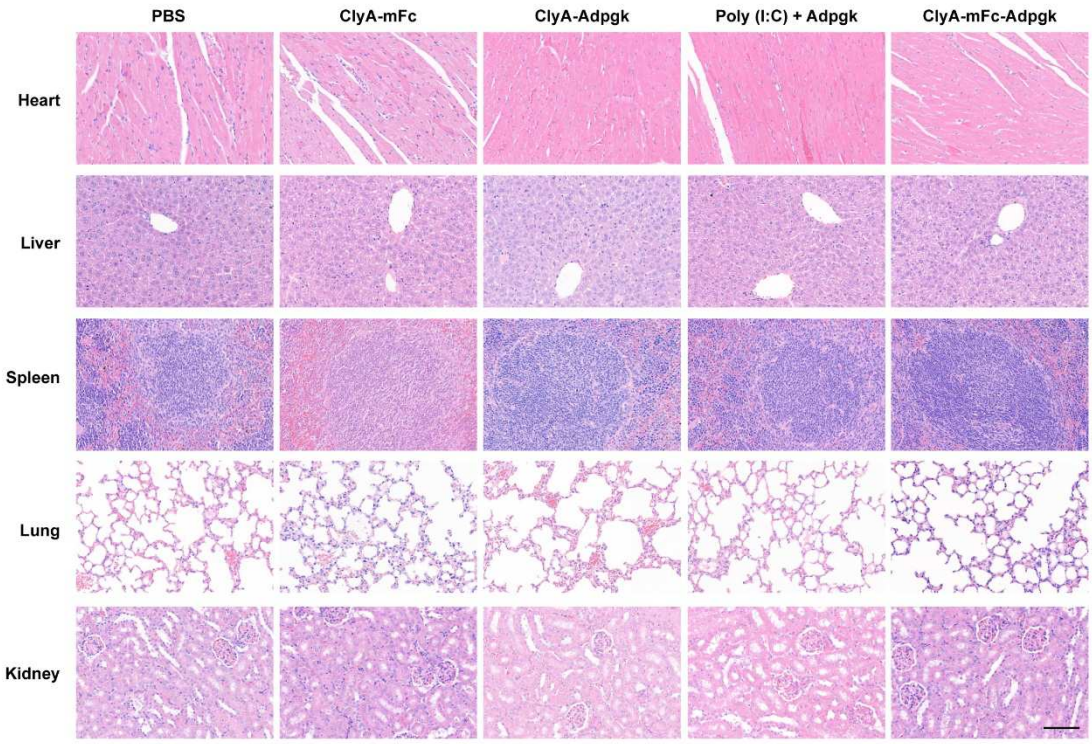

Supplementary figure 8 I H&E staining of major organs at the end of the experiment in the subcutaneous MC38 tumor model. Scale bar, 100 μm.

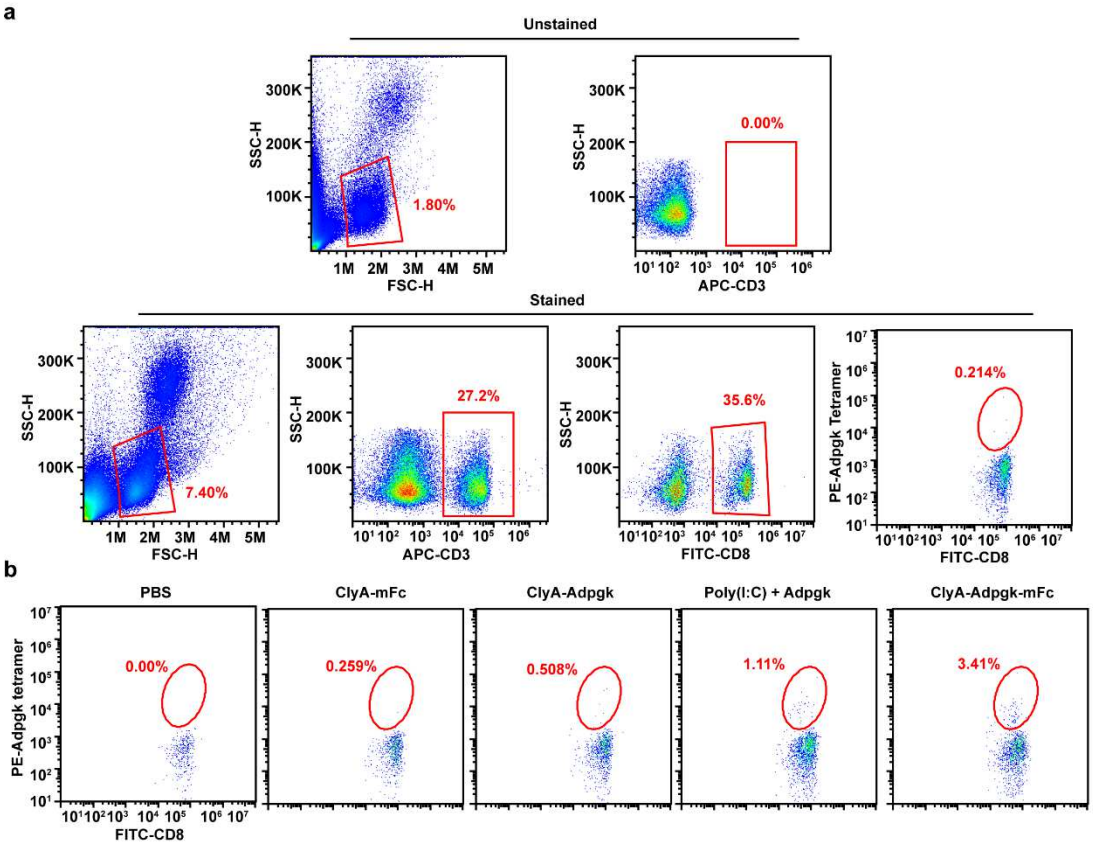

Supplementary figure 9 l Analysis of Adpgk tetramer^{+} in CD3^{+}CD8^{+} cells in the blood using flow cytometry at the end of the experiment in the subcutaneous MC38 tumor model (cf. Figure 5e). **a,** Gating strategy. **b,** Representative flow cytometry dot plots.

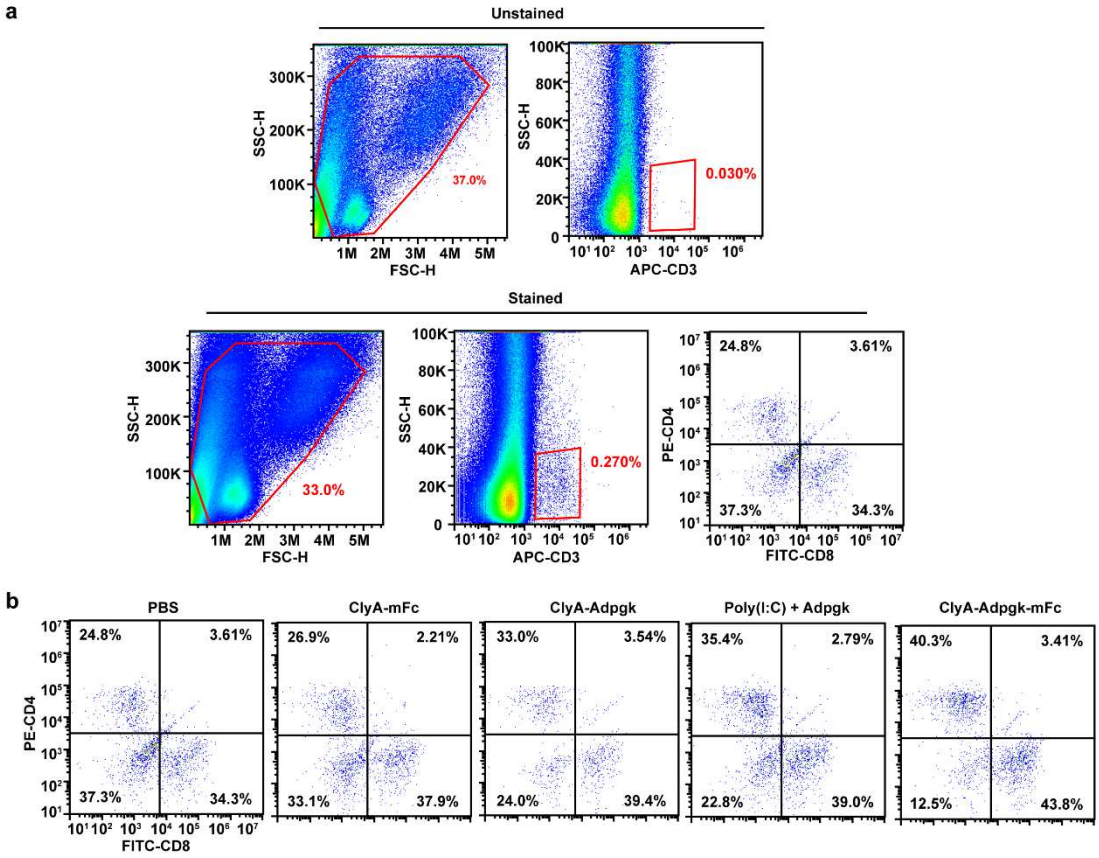

Supplementary figure 10 l Analysis of CD3^{+} T cells, CD3^{+}CD4^{+} T cells and CD3^{+}CD8^{+} T cells in tumor tissue using flow cytometry at the end of the experiment in the subcutaneous MC38 tumor model (cf. Figure 5h). **a,** Gating strategy. **b,** Representative flow cytometry dot plots.

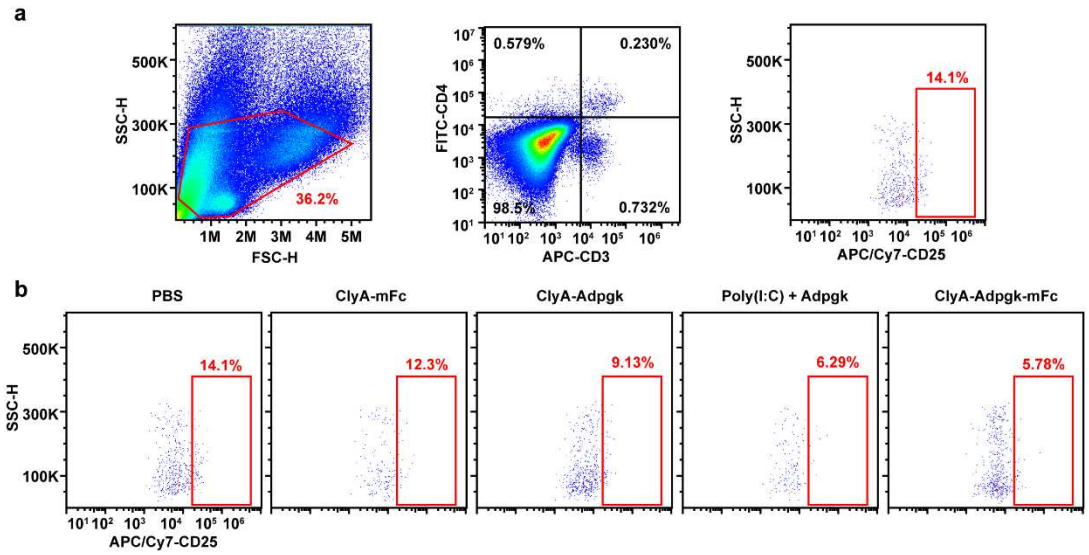

Supplementary figure 11 I Analysis of CD3⁺CD4⁺CD25⁺ Tregs in tumor tissue using flow cytometry at the end of the experiment in the subcutaneous MC38 tumor model (cf. Figure 5h). **a,** Gating strategy. **b,** Representative flow cytometry dot plots.

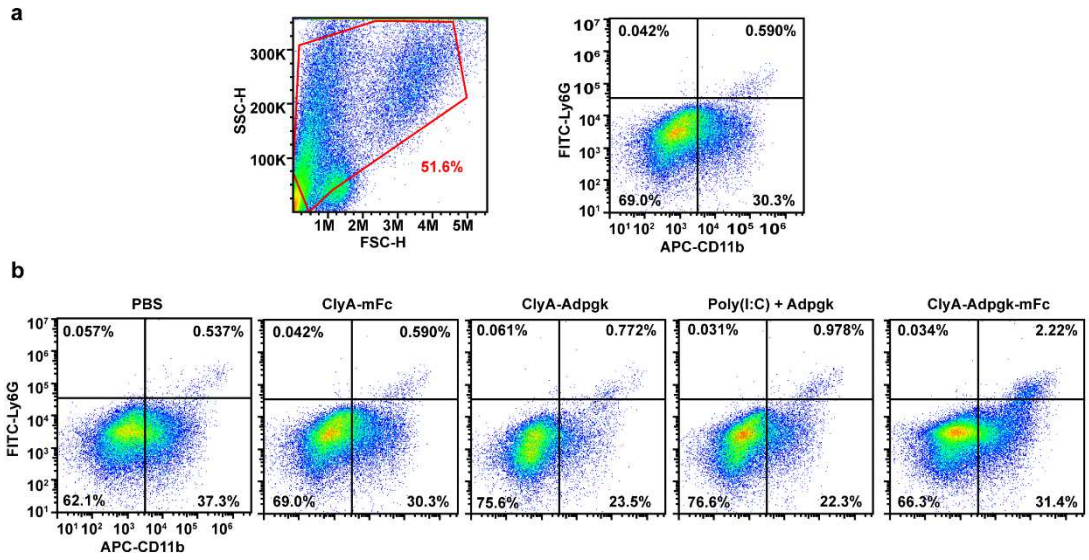

Supplementary figure 12 I Analysis of CD11b⁺Ly6G⁺ activated neutrophils in tumor tissue using flow cytometry at the end of the experiment in the subcutaneous MC38 tumor model (cf. Figure 5h). **a,** Gating strategy. **b,** Representative flow cytometry dot plots.

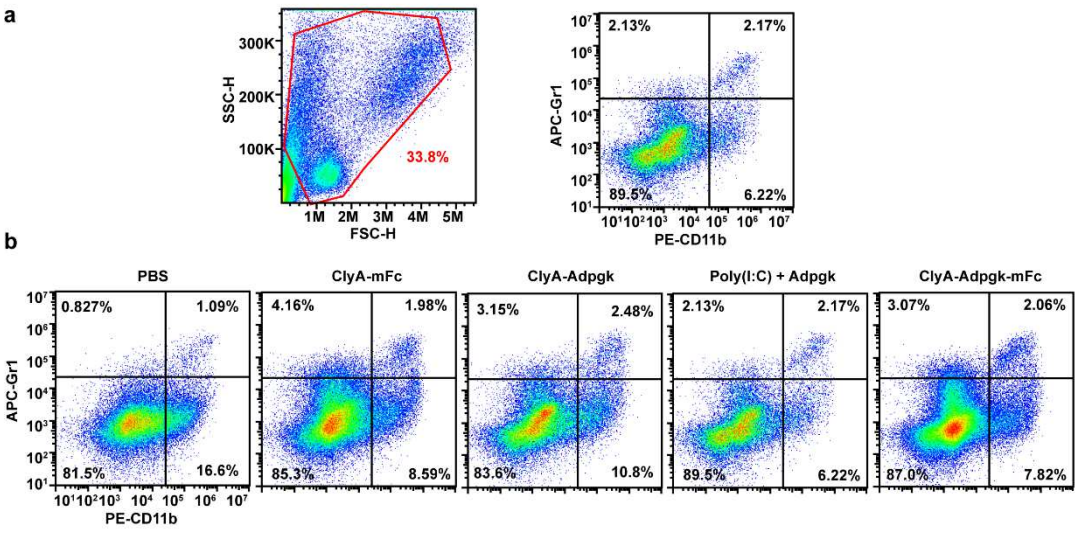

Supplementary figure 13 I Analysis of CD11b+Gr1+ MDSCs in tumor tissue using flow cytometry at the end of the experiment in the subcutaneous MC38 tumor model (cf. Figure 5H). **a,** Gating strategy. **b,** Representative flow cytometry dot plots.

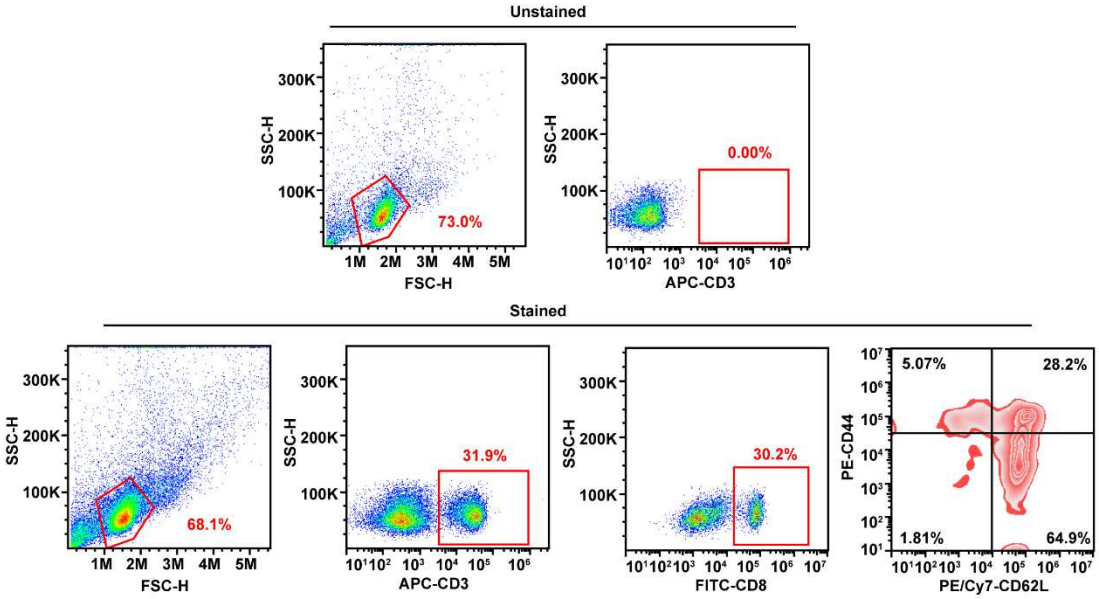

Supplementary figure 14 I Gating strategy of effector memory T cells (CD3+CD8+CD44+CD62L-) and central memory T cells (CD3+CD8+CD44+CD62L+) measured by flow cytometry in the immune memory analysis (cf. Figure 6b).